2019-01-01

Conductivity Modulation In Strained 2D Transition- Metal- Dichalcogenides Via Micro- Electro- Mechanical Actuation

Aldo Ivan Vidaña
University of Texas at El Paso

CONDUCTIVITY MODULATION IN STRAINED 2D TRANSITION- METAL-DICHALCOGENIDES VIA MICRO- ELECTRO- MECHANICAL ACTUATION

ALDO IVAN VIDAÑA

Master's Program in Electrical Engineering

APPROVED:

David Zubia, Ph.D., Chair

Jose Mireles Jr., Ph.D.

Robert C. Roberts, Ph.D.

David A. Roberson, Ph.D.

Stephen Crites, Ph.D.
Dean of the Graduate School

Dedication

I dedicate this thesis to my family, professors, and friends.

CONDUCTIVITY MODULATION IN STRAINED 2D TRANSITION- METAL-DICHALCOGENIDES VIA MICRO- ELECTRO- MECHANICAL ACTUATION

by

ALDO IVAN VIDAÑA, B.S.M.M.E.

THESIS

Presented to the Faculty of the Graduate School of

The University of Texas at El Paso

in Partial Fulfillment

of the Requirements

for the Degree of

MASTER OF SCIENCE

Department of Electrical and Computer Engineering

THE UNIVERSITY OF TEXAS AT EL PASO

August 2019

Acknowledgements

This is a fun yet difficult section to write. I will start where my passion for research at UTEP really began. I would have never decided to do research if it wasn't for Prof. John McClure course on Electronic Materials. Somehow he would always go on a tangent during lecture to talk about his solar cell research project which I thought it was funny yet very interesting. I will always remember that "balls roll downhill!" One day I decided to ask him if he had any positions available and that's is when he introduced to the NanoMIL group lead by Prof. Zubia. That is when I met a very productive group of students which convinced me to stay. I want to thank Dr. Brandon Aguirre, Ivonne Chavez, Dr. Jose Chavez, Damian Marrufo, and Dr. Arka Talukdar for being patient and for sharing their knowledge with me even though I had no idea what I was doing. This is when I got assigned my first mentor, Damian Marrufo. He was also so patient with me and thought me almost everything I needed to know about the project and solar cells in general. He showed me the pveducation.org webpage which tremendously helped me to understand the physics behind solar cells.

I also want to thank my friend and co-worker Dr. Rodolfo Aguirre aka el Rudy. Rudy was always there to help me understand difficult concepts related to my classes, whenever I encountered problems with tools in the lab he somehow always knew what was wrong with it, and also gave me very helpful personal advices. He thought me that mentors/graduate students are people too, and that it is normal to have fun once in a while. I have enjoyed spending time at many good music shows, dinners, and evening at bars with him.

The next person I also owe a serious debt is Dr. Sergio Almeida. One day he and Jose dragged me to my first biking adventure. Damian had left his mountain bike (it was a bit too big for me) in the office and they told me it would be ok if I borrowed it and went with them. I suffered a lot going uphill and down the Franklins but it sparked what became the driving force for progress and adventure in my life. Himself being a family man thought me a lot about the world and how to have a well-balanced life. Discussions with him were always intense and very honest. His

knowledge and intelligence always surprised me and always told me what I needed to hear along with effective criticism of dumb ideas. His research energy in combination with his never ending ideas always left me feeling ambitious to keep improving. Bike riding with him was always fun in El Paso and in the Bay Area, and I hope we get the chance to ride together again soon.

My time at UTEP has been tremendously shaped and influenced by many people, but no one has helped and thought me more like Prof. David Zubia has. I remember my first project with him began by doing a "jale chicano" (homemade) exhaust piece for one of the CSS tools in the cleanroom, which up to now it is still there. Then I was able to perform my first research experiments which involved using toxic materials and chemicals and I always felt so cool using them (maybe because the series Braking Bad was very popular back then). This work was very unique for me because apart from experimental work, I was allowed to help in the installment of several material depositors, wet benches, and characterization tools inside the new cleanroom facility which gave me valuable hands- on experience. Also, he provided me with life changing opportunities to work in various places such as Santa Barbara, CA, Grenoble, France, and Berkeley, CA which it helped me gain a new set of skills around my adaptability and cultural factors. His exceptional guidance both personally and professional have made me a better scientist and person overall. I could go on about how amazing he is but there are not enough pages in this thesis to thank him sufficiently. I am forever grateful.

My riding friends, my team members from Ep Cyclist, and my crazy friends from the HellPaso Bicycle Club for making Mondays more bearable. They played a huge role during grad school for keeping me happy with my life even in my worse moments. I believe they were one of the single most important key to success these past few years. Cycling makes me really happy and it is the ultimate path to happiness in life.

Last but not least, I want to thank my family for being supportive at all times even when things were not ok at home. I would of have never been here if it was not for them. For me family is everything and I did this for them.

This work was funded by National Science Foundation Award ECCS-0939514.

Abstract

In this thesis, strain-induced conductivity modulation in bi-layer molybdenum disulfide (MoS_2) flakes is experimentally investigated and modeled. Uniaxial tensile strain in the MoS_2 flakes is achieved using a micro-electro-mechanical (MEM) actuator. Conductivity ratios up to 400 are demonstrated. Theoretical predictions of conductivity versus applied voltage in the MEMS-MoS_2 device match experimental data reasonably well using only the effective width of the TMDC flakes as the sole fitting parameter. The amount of strain induced in the MoS_2 flakes was determined to be as high as 2.7% for one flake using the model fitted to the experiment data. The switching energy required to achieve a conductivity increase of 10^6 is calculated as a function of device critical dimension (length of TMDC flake). The model, which takes van der Waals forces into account, predicts a switching energy of 0.34 aJ/nm^2 and subthreshold swing of 17 mV/dec for a device scaled down to 10 nm. Since the cantilever MEMS design was not specifically made to strain TMDC flakes, the overall fabrication yield was poor. As a result, a new MEMS actuator was designed and fabricated to strain TMDC flakes more effectively at lower actuation voltages.

A poly-$Si_{0.35}Ge_{0.65}$-based MEMS comb-drive actuator was designed and fabricated using a CMOS compatible standard process to specifically strain a bi-layered (2L) MoS_2 flake and measure its electrical properties. Experimental results of the MEMS-TMDC device show an increase of conductivity up to three orders of magnitude by means of vertical actuation using the substrate as the gate terminal. A force balance model of the MEMS-TMDC was used to determine the amount of strain induced in the MoS_2 flake. Strains as high as 3.3% is reported.

Table of Contents

List of Figures

List of Tables

Chapter 1: Introduction & Motivation

1.1 CMOS Power Crisis

Over the last five decades, integrated-circuit (IC) manufacturers have followed Moore's Law by scaling down the size of the silicon-based transistors that are used as miniature electronic switches in digital computing chips [1]. At first, scaling all devices dimension had been sufficient to keep improving performance, until the submicron regime was reached. As the density of transistors in the most advanced ICs has increased over time, chip heat dissipation has become a major challenge [2, 3, 4]. Concurrently, cloud computing, social networking, mobile internet, and data analytics has steadily increased demand for information processing. These two things together have created an energy consumption problem for digital computing. Among many challenges encountered, the power crisis emerged mainly due to the fundamental operating principle of the MOSFET itself.

CMOS power consumption can be reduced by decreasing V_{DD} and scaling V_{TH} proportionally in order to maintain the same performance [5, 6]. However, a critical challenge is that when the operating voltage of a chip (V_{DD}) is reduced, the transistor on/off current ratio degrades. This can be observed in Figure 2, which shows the drain voltage and threshold voltage as a function of technology node [5, 2]. Voltage scaling began with the invention of the 90 nm technology shown in Figure 2. Additionally, since CMOS device dimensions are also scaled down, the leakage power density in CMOS devices has been increasing to the point that it is now comparable to active power density as shown in Figure 1 [2]. Power density in chip design has become a fundamental obstacle. For this reason, parallel processing (i.e. multi-core processors) was adopted to avoid the chip power density crisis [6]. However, this technique will ultimately not be sufficient due to the fundamental limit in CMOS energy efficiency.

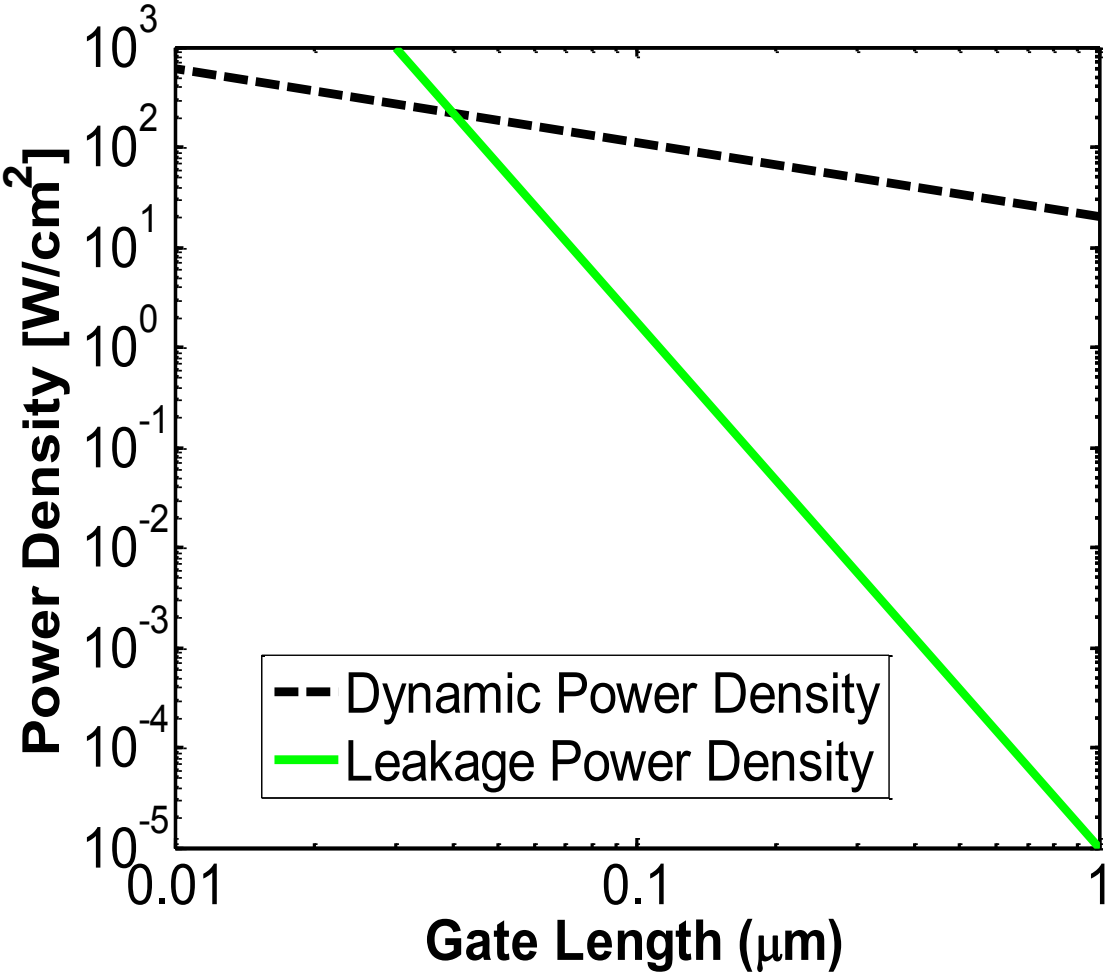

Figure 1: Chip power density vs. MOSFET gate length adapted from (adapted from [2]) As gate length reduces the leakage power density eventually surpasses the dynamic power density.

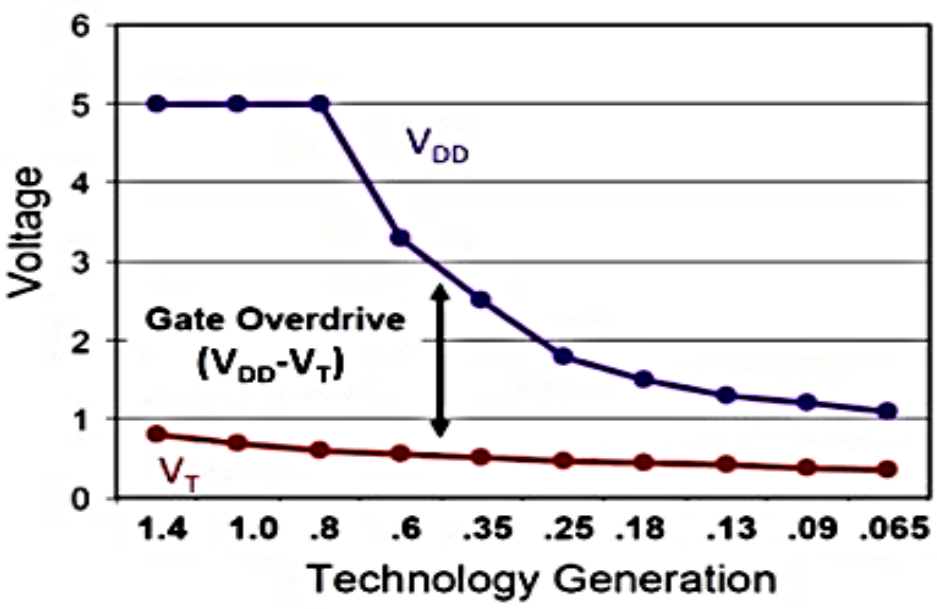

Figure 2: Historical supply voltage and MOSFET threshold voltage scaling [2].

A MOSFET is known to be an electronic switch that can be turned on by applying a voltage difference between the gate and the source (V_{GS}) [5]. The gate voltage at which conduction takes places is known as the threshold voltage (V_T). The typical drain current (I_D) vs. gate voltage (V_G) characteristic of MOSFET device is shown in Figure 3. When V_{GS} surpasses V_T, a conducive path of mobile charge carriers forms in the channel region allowing current to flow between source and drain. Hence, the on- current (I_{ON}) of a MOSFET is defined with the following equation:

$$I_{ON} \propto \mu_{eff} C_{ox} \frac{W}{L} (V_{DD} - V_T)^2 \qquad (1)$$

where μ_{eff} is the effective carrier mobility, C_{ox} is the gate oxide capacitance per unit area, W is the transistor gate width and L is the gate length.

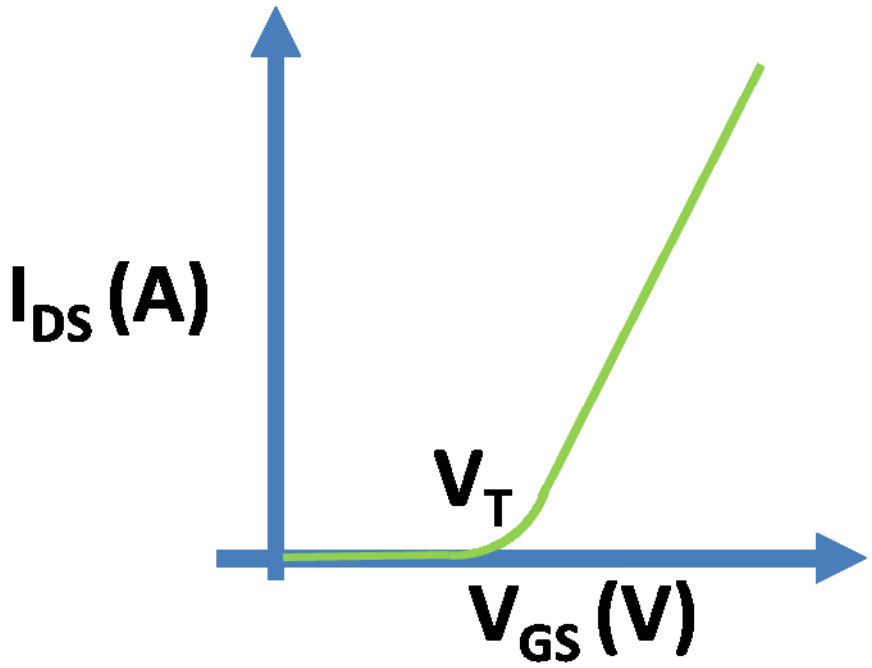

Figure 3: Drain current (ID) vs. gate voltage (VG) characteristic of MOSFET device

If I_D is plotted on a logarithmic scale vs. V_G (Figure 4), the off-state to on-state transition can be observed to be gradual and not abrupt. As V_{TH} decreases, the off-state leakage current (I_{OFF}) between the drain and the source increases exponentially and is set by non-scaling physical constants

$$I_{OFF} \propto 10^{\frac{-V_T}{SS}} \qquad (2)$$

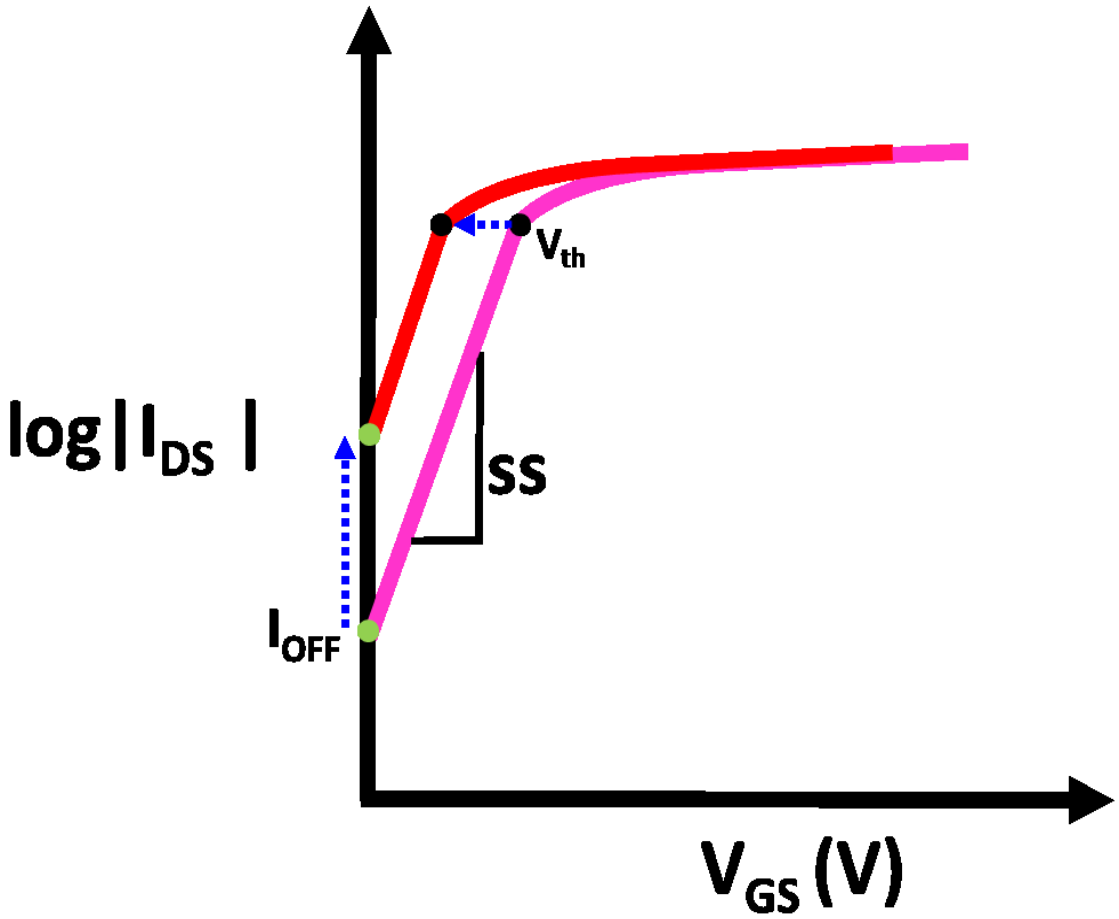

Figure 4: Transfer characteristic of an n-channel MOSFET (semi-log plot).

where the subthreshold swing (SS) is the inverse slope of the $\log(I_D)$- V_G curve. In practice, SS is typically around 100mV/decade, and is limited to be no less than (kT/q) x ln(10), which is 60mV/decade at room temperature. The value kT/q represents the thermal voltage and since it is a non-scaling physical constant, it results in a minimum energy limit for CMOS technology. Consequently, both the dynamic energy (proportional to V^2_{DD}) and leakage energy (proportional to I_{OFF} and V_{DD}) per unit area have increased.

One thing to note is that the voltage signal levels currently used in digital ICs are approximately 5 orders of magnitude higher than the Johnson noise levels in the metallic wires that transfer the signals [7, 8]. This mean that the signal voltage can be reduced by 10^2 times, which in turn decreases the energy needed to charge and discharge the wires by $\sim 10^4$. This effect happens because the energy scales as the square of the voltage, while maintaining good signal-to-noise ratio [8]. One way to ensure low standby power dissipation, is by maintaining a sufficiently large transistor on/off current ratio ($\sim 10^6$). Thus there is a need for new switch designs that can achieve high on/off current ratio with much smaller voltage signal [9].

Chapter 2: Technical Background

2.1 MICRO/NANO- ELECTROMECHANICAL SWITCHES (M/NEMS)

An electrostatic switch is usually composed of a movable electrode and a fixed electrode to form a capacitor. If a critical voltage is applied to the capacitor, there will be an electrostatic force between the electrodes large enough to bring the movable electrode to a critical distance ($g>g_0/3$) where there will be an instability that will bring it in contact with the fixed one, allowing current flow (Figure 5). If the actuating bias is removed, the device may passively switch back to the off-state due to the spring restoring force. Analytically this can be described by the sum of forces at equilibrium, which is given by,

$$\sum F = F_{sp} - F_{es} = 0. \quad (3)$$

Where F_{sp}, is the spring restoring force and F_{es} is electrostatic force. Furthermore, F_{es} given by coulomb's law is expressed as:

$$F_{es} = \frac{\varepsilon_r A V_G^2}{2(d-x)^2}, \quad (4)$$

where ε_r is the relative permittivity, V_G is the gate voltage. A is the actuation area in the movable beam, d is the distance or gap between the movable beam and the fixed gate, x is the displacement of the beam caused by the electrostatic force. The spring restoring force of the beam when an equally distributed force is applied uniformly across the beam is given by the following formula [10]

$$F_{sp} = k_s x = \left[\frac{2EW^3 t}{3L^3}\left[\frac{3}{8-6(L_C/L)+(L_C/L)^2}\right]\right] x, \quad (5)$$

where E is the Young Modulus of the structural material, L is the total length of the beam, L_C is length of the portion of the beam in which the electrostatic force is applied, W is the beam width,

and t is the thickness. As a result, by combining equations (3)-(5), the gate voltage can finally be expressed as:

$$V_G = \sqrt{\frac{2k_s x(d-x)^2}{\varepsilon A}}. \tag{6}$$

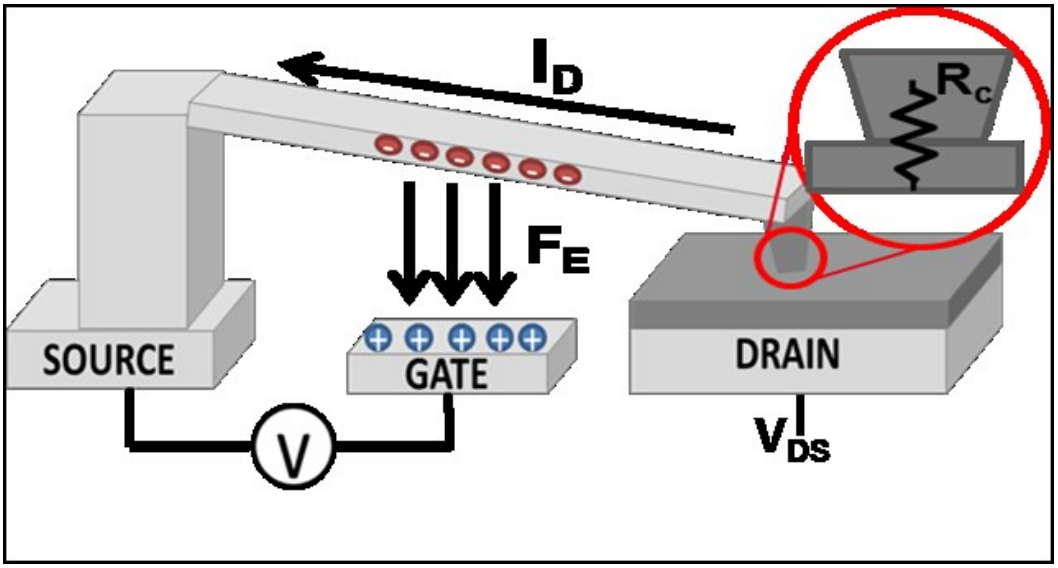

Figure 5: Schematic illustration of a MEM relay in the ON state. The voltage between the gate (fixed plate) and source (movable beam) induces and electrostatic force large enough to bring the movable beam into contact with the drain (fixed) allowing current to flow.

Electromechanical devices possess extremely steep switching behavior and essentially zero off-state leakage (I_{OFF}) as shown in Figure 6 which then free the devices from the limitations dictated by subthreshold leakage [11]. The energy per operation for mechanical relays are predicted to be lower than the energy per operation for CMOS technology. This advantage stems from being able to scale down the threshold and supply voltages without increasing the off-state current [11, 6].

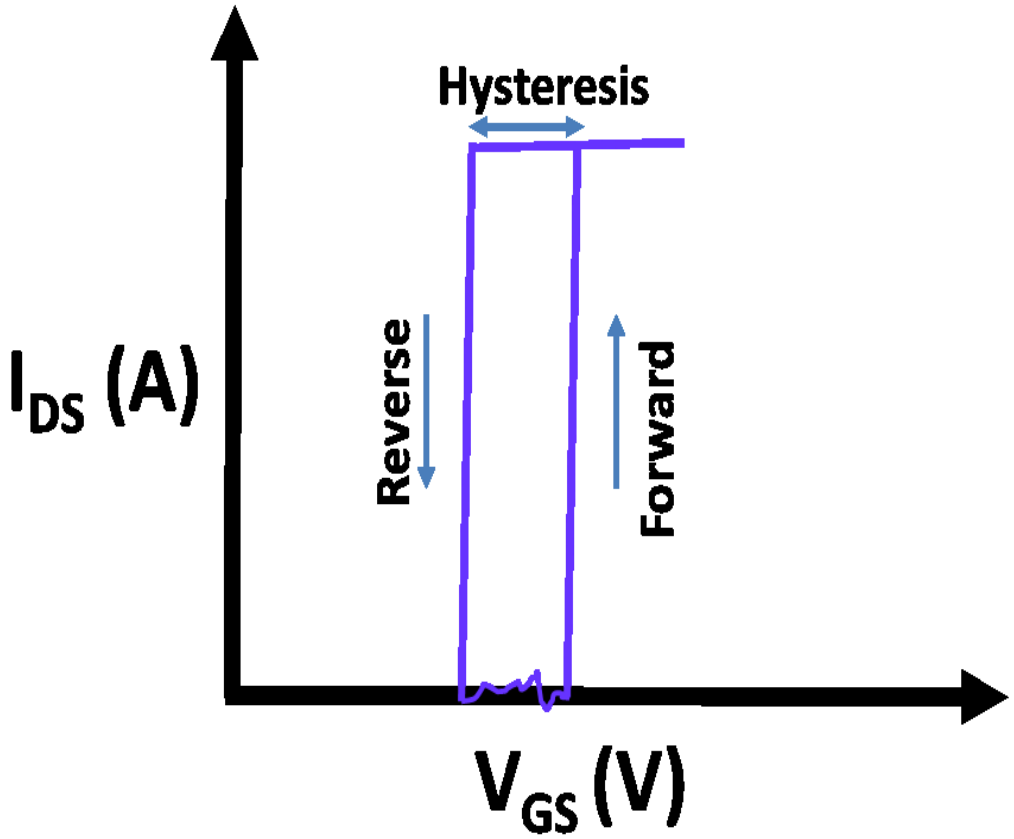

Figure 6: Voltage-Sweep Showing Transfer characteristics of a MEM relay. Hysteresis behavior is typical due to the natural occurring forces of adhesion between two contacting surfaces.

As a result of the MOSFET energy efficiency limit, M/NEMS devices have been proposed as an alternative switching device for digital logic. M/NEMS devices can be classified accordingly to their actuation mechanism. These include magnetic, thermal, piezoelectric, and electrostatic actuators [12]. M/NEMS switches that work with the electrostatic actuation mechanism are of interest since they can be fabricated using relatively standard surface micromachining techniques and materials. They also are more scalable and do not consume substantial active power [13] [6] [14].

As promising as these devices look, there are still many present challenges that exist. For example, low contact reliability and limited endurance. Stiction is another major problem in

M/NEMS devices [12]. Stiction occurs when the surface adhesion forces become higher than the spring restoring force. As a result, the device may be permanently stuck in the On-State. This may be caused by micro-welding, or surface area increase caused by plastic deformation. Therefore, contact materials with high melting point, high hardness, or low adhesion energy are needed to avoid this problem. Conversely, an abrupt increase in contact resistance (*e.g.* due to oxidation or friction polymers) may cause the device to appear permanently in the Off- State. As a result, materials featuring a thin passivation layer or high oxidation resistance properties will be needed. Finally, material transfer occurring between the contacting anode and cathode may lead to either permanent ON or OFF failures. This behavior can possibly be mediated by field emission effect across nano- gaps which would be enhanced by a large roughness of the contacting surfaces.

Recent works have demonstrated that using molecular coatings between the contacting surfaces will yield a lower surface energy resulting in a smaller hysteresis [15]. This is achieved by filling the gap between the contacts with a specific organic molecule which is then compressed until the point that current is able to pass through by a mechanism known as tunneling. Current research is now being focused on using different filler materials to lower the operational voltage of the MEMS.

2.2 TWO-DIMENSIONAL TRANSITION-METAL DICHALCOGENIDES (TMDCS)

Two-dimensional layered materials such as transitional metal dichalcogenides (TMDCs) have received much interest lately due to their unique and useful properties. Much research is being performed to study their material, optical, and electronic properties and also how they can be used in practical devices. Two-dimensional layered materials consist of in-plane covalent/ionic bonding with van der Waals interlayer interactions. Unlike graphene, many 2D layered materials

are semiconductors. These include TMDCs (e.g. MoS_2, WSe_2), other layered dichalcogenides (e.g. SnS_2, $SnSe_2$), and black phosphorus (BP).

A TMDC monolayer consists of three atomic layers in which the transition metal is covalently bonded by two chalcogens in a sandwich-like structure as shown in Figure 7 [16]. The weak van der Waals interactions between adjacent planes permit isolation of monolayers from the bulk using mechanical or chemical exfoliation methods. Monolayers of TMDCs have very distinct electrical properties from their bulk counterparts, primarily due to the confinement of charge carriers in two dimensions [16]. Furthermore, monolayers possess atomic scale smoothness and they have virtually no dangling bonds or defects which explains their exceptional mechanical properties such as very high tensile strains.

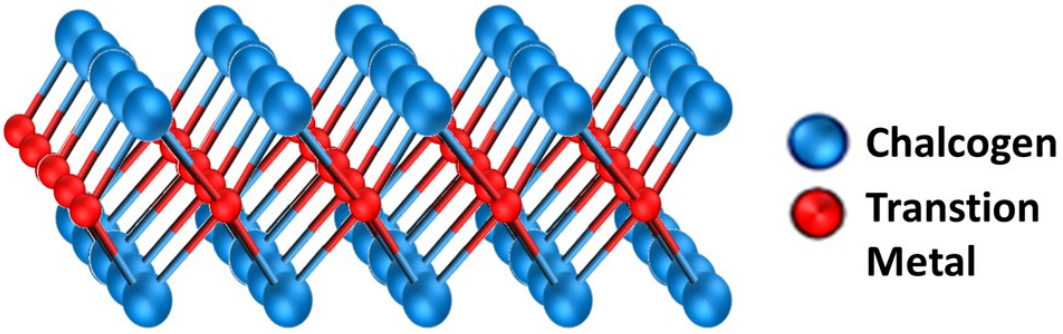

Figure 7: TMDC monolayer molecule with a sandwich-like structure in which the transition metal (red atom) is covalently bonded by two chalcogens (blue atoms).

One property of particular interest, called “deformation potential”, is the change in band gap due to mechanical strain. For example, the bandgap of MoS_2 in its monolayer form is predicted to decrease to zero when subjected to 11% tensile strain [17] as shown in Figure 8. Additionally, MoS_2 has shown exceptional strength with a fracture point at 11% tensile strain [18]. Deformation potential has been explored for various applications including: flexible electronics, strain-engineered photovoltaics, and strain sensors [19, 20, 21, 22, 23].

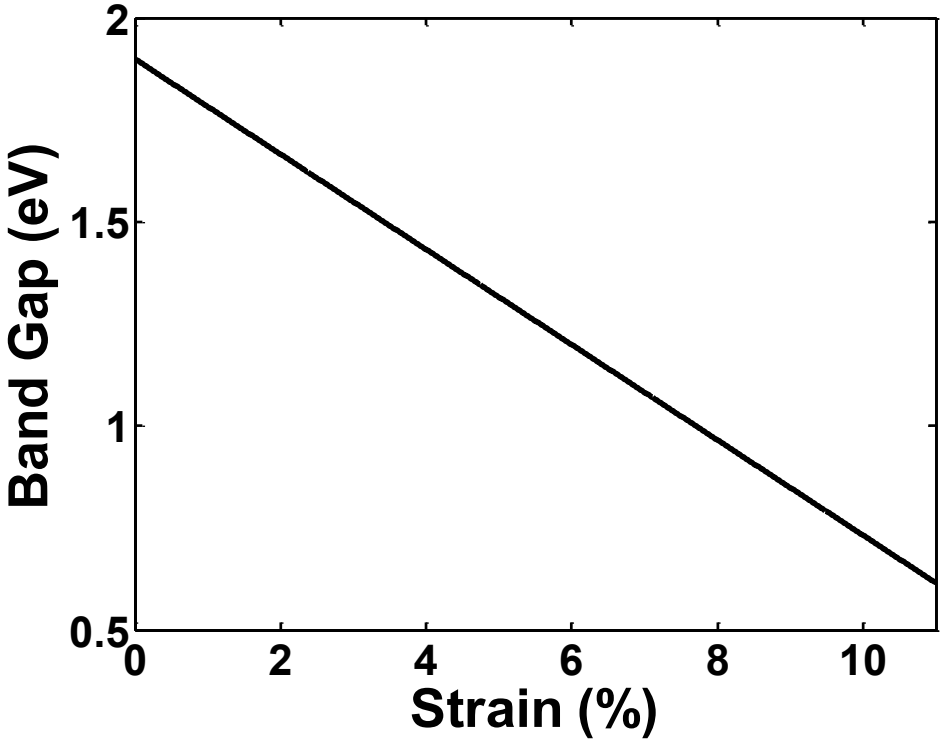

Figure 8: Band gap change as a function on tensile strain in bi layered MoS_2.

Chemical vapor deposition (CVD) has been one of the most common methods to yield large-area and high quality TMDCs monolayers [24]. Fundamentally, this process can be quite simple. In this process, usually SiO2/Si or sapphire substrates are placed inside a vacuum chamber quartz tube. Then, solid precursors such as MoO_3 and S are place inside the furnace using boats made out of ceramic, alumina (Al2O3), graphite, or even tungsten. These precursors are then heated until the material vaporizes, allowing them to react with each other and settle onto the substrate material to form monolayers.

Another method is using mechanical exfoliation, which was proposed in 2004. Currently, it is one of the most used techniques due to the weak van der Waals forces between layers in TMDCs that allows isolation single-monolayers possible [25]. Micromechanical exfoliation

involves repeatedly peeling a TMD crystal using adhesive tape until a monolayer is obtained and then transferred onto a desired substrate.

2.3 2D TMDC-MEMS TRANSISTOR - THE 'STRITCH'

Recently, the deformational potential of TMDCs was proposed for ultra-low power switching devices [26, 27, 28]. The idea combines both using MEMS and TMDC thin layers to overcome the CMOS power crisis. The proposed device works on the key concept of reducing the bandgap (hence increasing conductivity) of a TMDC thin layer by means of strain using a MEMS actuator. The way this device works is illustrated in Figure 9, where a thin layer of TMDC is suspended and clamped between a moveable beam (source) and a fixed stud (drain). In the OFF state, there is a small constant voltage applied between the source and drain (V_{DS}) but there is no voltage applied between the gate and the source so the bandgap is still large, allowing only a very small current to pass through. However, when the gate voltage is increased, the electrostatic force will attract the movable beam towards it and will uniaxially strain the TMDC as shown in Figure 9.bii. The strain on the TMDC causes a bandgap reduction and allows electrical current to pass between the drain and source, so the device is now in the ON state as shown in Figure 9.cii [27]. The theoretical model and first experimental proof of concept results were published in the IOP Semiconductor Science and Technology Journal [28].

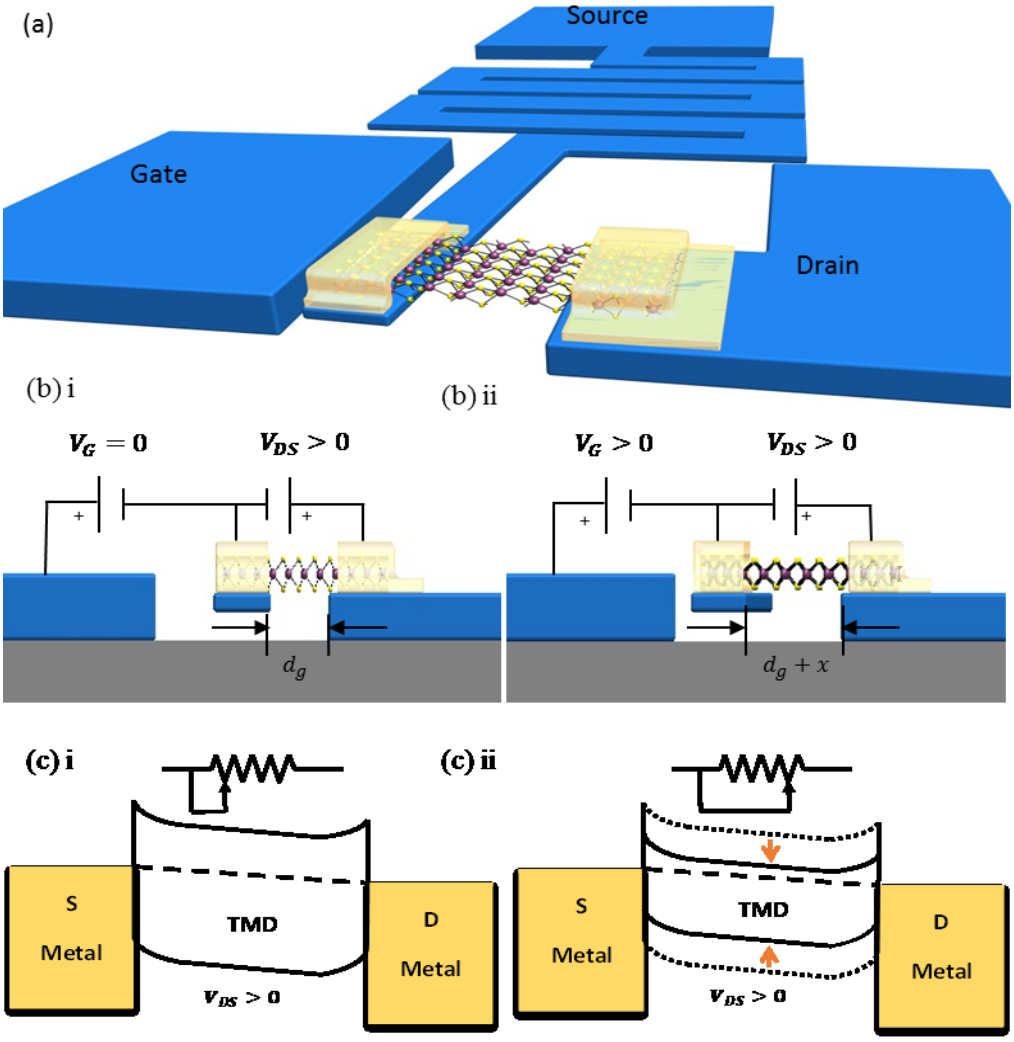

Figure 9: (a) Isometric view of the device at On state, (b) and (c) crosssectional view of the device at Off and On state respectively [27] .

Chapter 3: Conductivity Modulation in Strained Transition-Metal-Dichalcogenides via Micro- Electro- Mechanical Actuation

3.1 INTRODUCTION

Over the last five decades, integrated-circuit (IC) manufacturers have followed Moore's Law by scaling down the size of the silicon-based transistors that are used as miniature electronic switches in digital computing chips [1]. As the density of transistors in the most advanced ICs has increased over time, chip heat dissipation has become a major challenge [2, 3, 4]. At the same time, the advent of cloud computing, social networking, mobile internet, and data analytics has steadily increased demand for information processing. These two trends together pose a growing energy consumption problem for digital computing. Fortuitously, the voltage signal levels currently used in digital ICs (0.8 V) are approximately 5 orders of magnitude higher than the Johnson noise levels in the metallic conductors (~8 μV) that convey the signals [7, 8]. This presents an opportunity to reduce the signal voltage by 10^2 times and the energy needed to charge and discharge the wires by ~10^4, since the energy scales as the square of the voltage, while maintaining good signal-to-noise ratio [8]. Equally important is maintaining a sufficiently large transistor on/off current ratio (~10^6) to ensure low standby power dissipation. Thus there is a need for new switch designs that can achieve high on/off current ratio with much smaller voltage signal [9]. Alternatively, micro/nano-electro-mechanical system (M/NEMS) devices [11] are known to have excellent on/off ratios with high steep transitions. However, stiction between the contacts is an issue and research has focused on using compressible materials and other coatings to improve reliability [15]. Lately, there has been remarkable progress on the exploration of two-dimensional layered materials, such as graphene and transitional metal dichalcogenides (TMDC) materials. Monolayers of TMDC materials have very distinct electrical properties from their bulk

counterparts, primarily due to the confinement of charge carriers in two dimensions [16]. Furthermore, combined with their excellent mechanical properties and ultra-low mass, TMDC materials have also been investigated for high frequency resonators. [21, 22] An important property of some TMDC materials is that their bandgaps (>1eV) are highly sensitive to strain, which make them excellent candidates for strain-based sensors [24, 23, 20]. The aforementioned property has also been explored in MoS_2 field effect transistors demonstrating improved device performance, such on-current increase. [29, 30]. Recently, the large deformation potential (coefficient of strain-induced change in semiconductor band-gap energy) exhibited by TMDC materials was proposed for low-energy switching, as a theoretical analysis predicted an on/off current ratio of 10^6 for an input voltage signal of 75 mV [27]. In this chapter, the change in conductivity with applied uniaxial strain in TMDC materials is first analyzed. A micro-electro-mechanical (MEM) actuator was then used to strain TMDC flakes, resulting in a large increase in their conductance. Moreover, a theoretical model is presented that predicts and closely matches the electrical characteristics of the MEMS-TMDC device. Finally, this chapter explores an energy-efficient means to induce strain in the TMDC flake by scaling down the MEMS-TMDC device to the nanometer regime. The transfer characteristics are presented and compared to an ideal MOSFET device.

3.2 Conductivity versus Strain in Transition-Metal Dichalcogenides

The influence of strain on the conductivity of a TMDC is presented in this section. Figure 10(a) and (b) show perspective views of a TMDC under zero and non-zero uniaxial strain, respectively. x_o is the equilibrium length of the TMDC at zero strain, x is the length under strain

and w is the width. From atomistic simulations [31], the influence of strain (and therefore lattice deformation) on the band-gap energy can be linearly approximated as

$$E_g(\varepsilon) = E_{g0} + \phi_{dp}\varepsilon \quad (7)$$

where E_{g0} is the band gap at zero strain, ϕ_{dp} is the deformation potential, and ε is the strain, defined by $\varepsilon = (x - x_o)/x_o$. Although the effective mass and mobility of electrons are also affected by strain [32], these effects are exponentially smaller than the effect of band-gap modulation and hence are not included in the analysis herein.

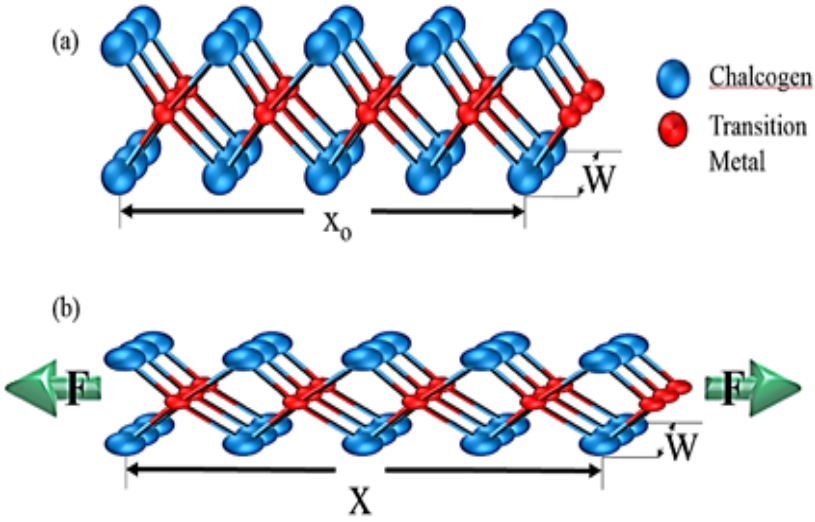

Figure 10: Schematic diagrams of a transition metal dichalcogenide monolayer in its a) relaxed state and b) under uniaxial tensile strain.

In this analysis piezoelectric effects can be ignored by using a bilayer (2L)-MoS_2 since the bilayer does not show piezoelectric effects [24]. Another assumption is that the contact between the TMDC and the metal is Ohmic (or has minimal Schottky barrier). MoS_2 has shown Ohmic contact with metals such as Au [33] and Sc [34]. Under these assumptions, the current flowing through the TMDC from drain to source is dominated by drift and expressed as,

$$I_{DS} = w_{TMDC}(q\mu_e n_{2D} + q\mu_h p_{2D})\mathcal{E}_{DS} = w_{TMD}\sigma_S\mathcal{E}_{DS} \quad (8)$$

where w_{TMD} is the TMDC width , q is the electron charge, and μ_e and μ_h are the electron and hole mobilities, respectively. For MoS_2, $\mu_e = 79$ $cm^2V^{-1}s^{-1}$ and $\mu_h = 194$ $cm^2V^{-1}s^{-1}$ [32]. n_{2D} and p_{2D} are the 2D electron and hole concentrations (cm^{-2}), and $\mathcal{E}_{DS}$ is the electric field between the source and drain. n_{2D} is given by,

$$n_{2D} = \int_{E_C}^{\infty} DOS_{2D} f(E) dE \qquad (9)$$

where $f(E)$ is the Boltzmann distribution, DOS_{2D} is the 2D density of states which can be express as,

$$DOS_{2D} = \frac{1}{\pi\hbar^2} \sum_{i=1}^{n} g_i m_i^* H(E - E_{Ci}) \quad (10)$$

$\hbar$ is the reduced Planck's constant, g_i is the valley degeneracy, m_i^* is the effective mass corresponding to each valley, and $H(E - E_{Ci})$ is the Heaviside unit step function. For TMDs, the valleys with energy above the first two levels can be neglected [35]. Thus the electron carrier concentration can be expressed as,

$$n_{2D} \approx \frac{kT}{\pi\hbar^2}\left(g_1 m_1^* + g_2 m_2^* \exp\left(-\frac{\Delta E_C}{kT}\right)\right) \exp\left(-\frac{E_C - E_F}{kT}\right) = N_{C_{2D}} \exp\left(-\frac{E_C - E_F}{kT}\right) \qquad (11)$$

where k is the Boltzmann constant, T is temperature, and ΔE_C is the difference between the two lowest valleys in the conduction band. In 2D TMDC materials several properties can be fine-tuned by just choosing the number of layers. Therefore, by considering the actual thickness of the TMDC through the DOS_{2D} and bandgap, n_{2D} and p_{2D} sheet carrier concentrations can be formulated. Thus, specifying the number of layers is essential to account for the thickness of the TMDC molecule. For a 2L-MoS_2, the lowest valley of the conduction band occurs at the K point giving a valley degeneracy $g_1 = 2$ with a $m_1^* = 0.579m_e$, whereas the second lowest valley occurs between the K-Γ points giving a degeneracy of $g_2 = 6$ with a $m_2^* = 0.542m_e$, and $\Delta E_C \cong$

69.3 meV [36]. In a similar way, the hole concentration, considering only the valley at the Γ point with an effective mass of $m_h^* = 1.168m_e$ [36], is given by,

$$p_{2D} \approx \frac{m_h^* kT}{\pi\hbar^2} \exp\left(-\frac{E_F - E_v}{kT}\right) = N_{V_{2D}} \exp\left(-\frac{E_F - E_v}{kT}\right). \quad (12)$$

Combining (11) and (12) under the assumption that a TMDC is intrinsic so that the electron and hole concentrations are equal to each other ($n_{2D} \approx p_{2D}$), the sheet conductivity can be expressed as

$$\sigma_S(\varepsilon) = q\sqrt{N_{C_{2D}} N_{V_{2D}}}(\mu_e + \mu_h) \exp\left(-\frac{E_g(\varepsilon)}{2kT}\right) \qquad (13)$$

where q is the electronic charge, $N_{C_{2D}}$ and $N_{V_{2D}}$ are the two-dimensional effective density of states in the conduction band and valence band, respectively, and μ_e and μ_h are the electron mobility and hole mobility, respectively. The conductivity of a TMDC therefore can be expressed in terms of the deformation potential and strain by substituting (7) into (13) to obtain

$$\sigma_S(\varepsilon) = \sigma_{S_O} \exp\left(-\frac{\phi_{dp}\varepsilon}{2kT}\right) \qquad (14)$$

where $\sigma_{S_O} = q\sqrt{N_{C_{2D}} N_{V_{2D}}}(\mu_e + \mu_h) \exp\left(-\frac{E_{g0}}{2kT}\right)$ is the strain-free sheet conductivity in units of Siemens. The level of strain required to increase the conductivity of the TMDC by a specified amount can be determined by solving Equation (14) for strain:

$$\varepsilon = \frac{-\ln(\sigma_S/\sigma_{S_O})2kT}{\phi_{dp}} \qquad (15)$$

Figure 11 plots the strain to strain-free conductivity ratio (σ_S/σ_{S_O}) of mono- (1L), bi- (2L), and tri- (3L) layer MoS_2 films as a function of tensile strain using the reported deformation potential for these thicknesses [37], up to the ultimate tensile strain of 11% for a mono-layer of MoS_2 [18]. From this plot it can be seen that a switching device using this material can achieve an on/off current ratio of 10^{11}, in principle. Their exponential dependence of conductivity on strain

and exceptional strength motivates the investigation of TMDC materials for switching applications.

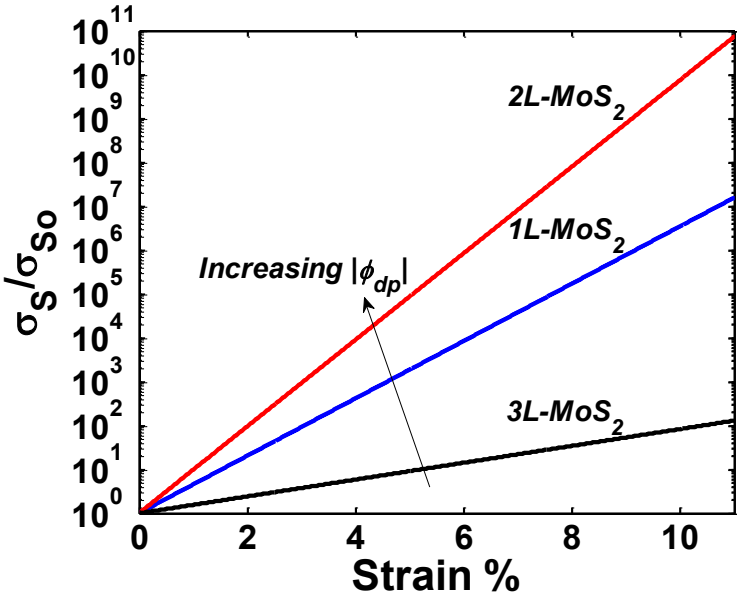

Figure 11: Normalized conductivity of MoS_2 films as a function of strain.

3.3 Experimental Conductivity of Strained 2L-MoS_2

In this experiment, pre-existing MEMS cantilever actuators were used to uniaxially strain MoS_2 flakes. The fabrication process of the MEMS is reported by Nuo Xu, Tsu-Jae King Liu, et al. elsewhere [38] . MoS_2 bi-layers were mechanically clamped and suspended between the fixed pad (drain) and movable beam (source) of the MEMS actuator. A voltage was then applied between the gate and source terminals to strain the 2L–MoS_2 flake and its conductivity was measured. 2L–MoS_2 was selected for this experiment due to its relatively large deformation potential.

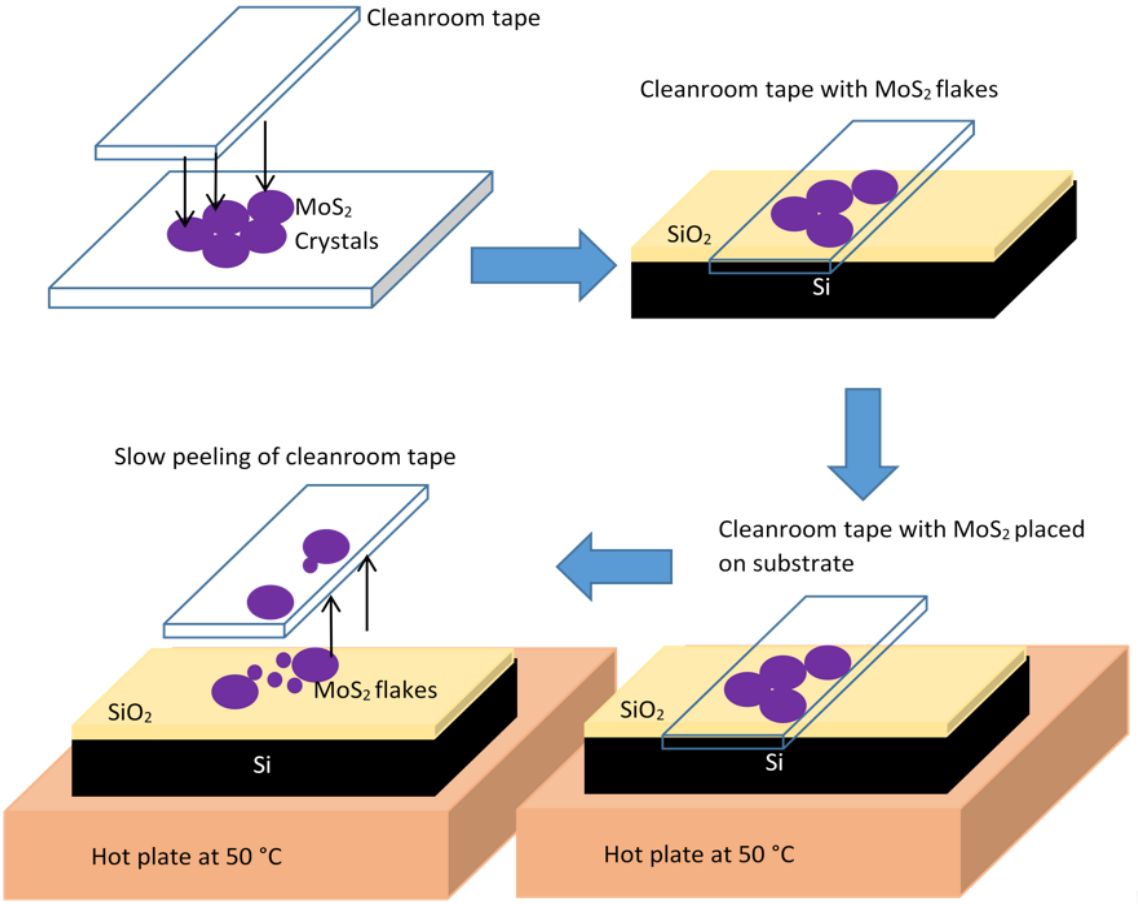

Figure 12: Schematic diagram of mechanical exfoliation of MoS_2 flakes using cleanroom tape and a hot plate at 50 °C.

The MoS_2 flakes were mechanically exfoliated from a rock source as shown in Figure 12. Cleanroom tape was used to transfer the TMDC flakes from the rock source to the substrate due to its minimal residue. The piece of tape with the TMDC flakes is then placed on a silicon substrate with an oxide (260nm for optical contrast) at 50 degrees Celsius (to get rid of air bubbles in the tape) and slowly peeled. Next, Raman/PL spectroscopy is utilized to verify the number of layers by analyzing the frequency difference between the two vibration modes as shown in Figure 13 [39]. In this case, a frequency difference of 21 cm^{-1} indicated that the MoS_2 flake was bi-layered.

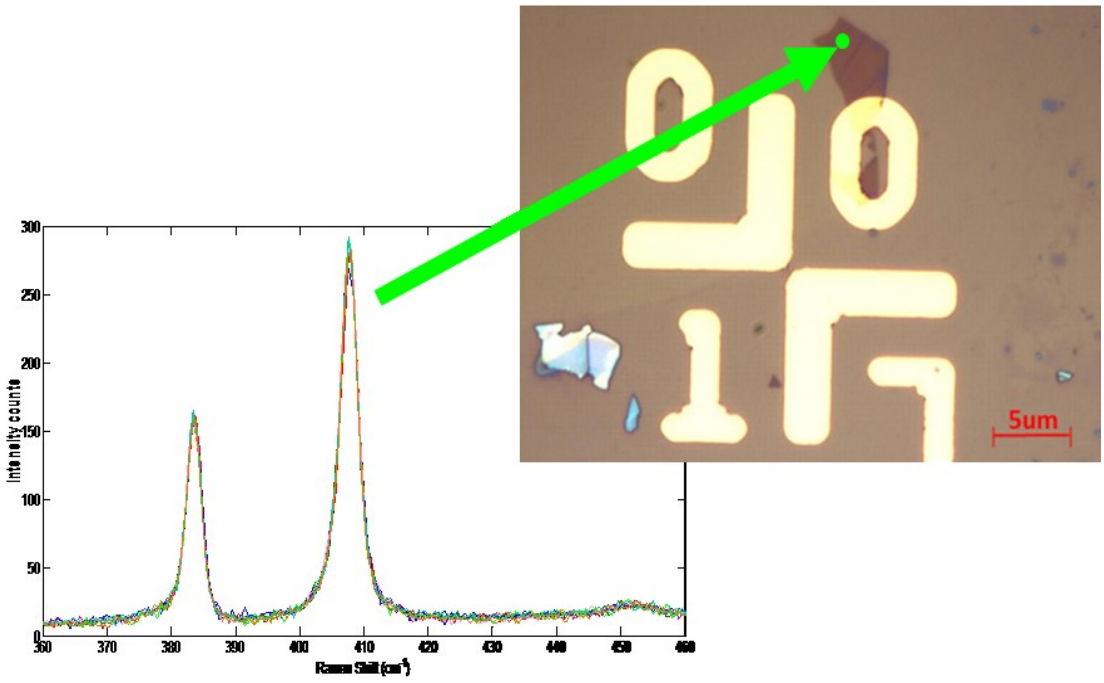

Figure 13: Raman Spectroscopy of 2L MoS_2 mechanically exfoliated on patterned SiO_2/Si substrate.

The MoS_2 flakes are then transferred onto the MEM actuator using poly(methyl- methacrylate) (PMMA) as the transfer medium as described in Figure 14 [40]. This process starts by spin coating PMMA A11 950 onto a SiO_2/Si substrate at 2000RPM followed by a heat treatment at 180 °C for 90 seconds. This step is done twice to achieve a thick (~4 um) PMMA layer. The next step is to cut PMMA slabs using a micro-engraver. Then using a micro- hook, the PMMA slab is picked up and placed on the desired TMDC flake. The substrate undergoes a heat treatment at 160 °C for 90 seconds so the TMDC flake adheres to the PMMA. Then the PMMA slab with the TMDC is picked up using the micro-hook and placed directly on the MEMS actuators followed by a heat treatment at 180 °C. Finally, the PMMA slab is dissolved using dichloromethane (DCM), which is a solvent similar to acetone but dissolves the PMMA in a less aggressive manner.

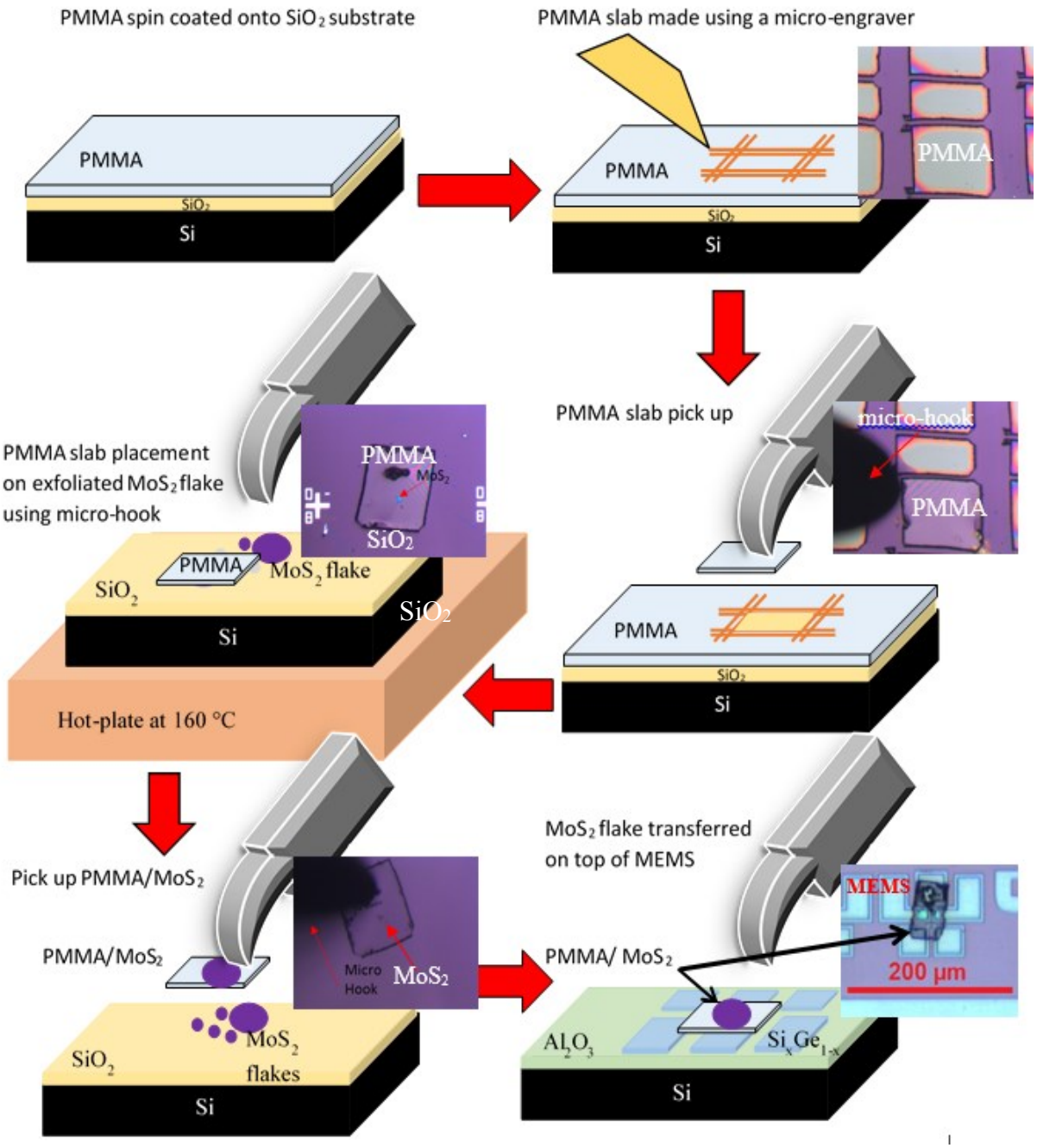

Figure 14: Schematic diagram with experimental optical micrographs of PMMA transfer process of a MoS_2 flake on top of a MEMS.

Mechanical clamping and electrical contacting of the MoS_2 flake to the poly-$Si_{0.35}Ge_{0.65}$ was achieved by deposition and patterning of Cr/Au via electron beam deposition and lithography using

a lift-off process. Gold was used for two reasons; MoS_2 with Au contacts have ohmic behavior (or minimal Schottky barrier) [41]; it has also been shown that sulfur atoms form semi-covalent bonds with Au atoms, creating a strong clamping mechanism [42, 43]. Finally, the cantilever beam was released by selectively removing an underlying sacrificial layer of SiO_2 using anhydrous vapor HF. Figure 15 shows optical microscope images of the device with a MoS_2 flake suspended between the movable source and fixed drain electrodes comprised of patterned poly-$Si_{0.35}Ge_{0.65}$.

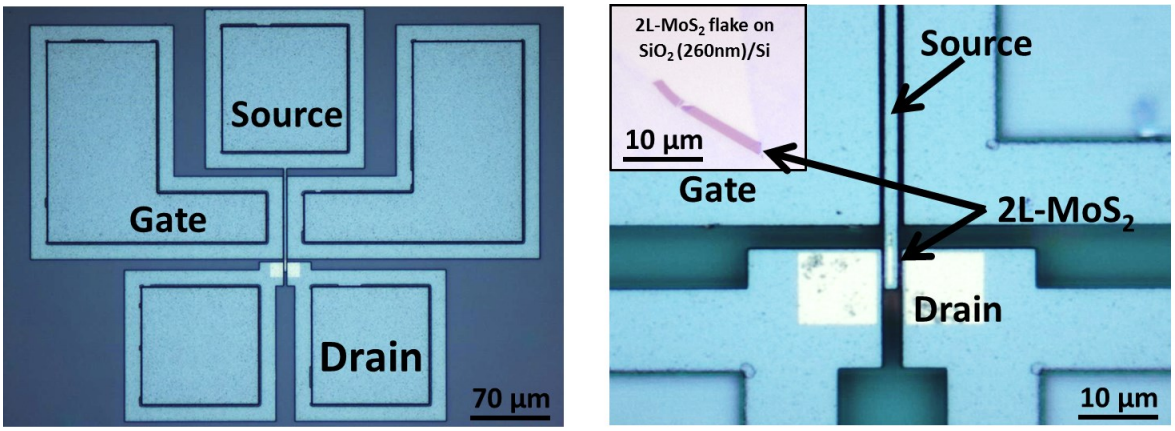

Figure 15: (a) Low- and (b) high-magnification optical microscope images of a fabricated MEMS-TMDC device with a bilayer MoS_2 flake. Inset shows MoS_2 flake #1 on a SiO2/Si substrate before it was transferred to the MEMS actuator.

Two independent devices were fabricated and tested by two different researchers using the same MEMS design but different actual MEMS actuators and MoS_2 flakes. Measured σ_S/σ_{S_O} versus V_{GS} characteristics of the two devices are plotted in Figure 16. The conductivity ratios of flake 1 (blue trace) and flake 2 (pink trace) increased to 400 and 20 when the applied gate voltages were increased to 28 V and 31.5 V, respectively. A constant voltage of 200 mV was applied between the drain and source in both devices. The dimensions and material parameters of the MEMS actuator and MoS_2 flakes are listed in the experimental column of Table 1. The tensile

strain induced in the MoS_2 films were calculated to be $\varepsilon_{TMD} = 2.7$ % and $\varepsilon_{TMD} = 2.1$ % for flakes 1 and 2, respectively, using Equation (15) and the measured σ_S/σ_{S_O}.

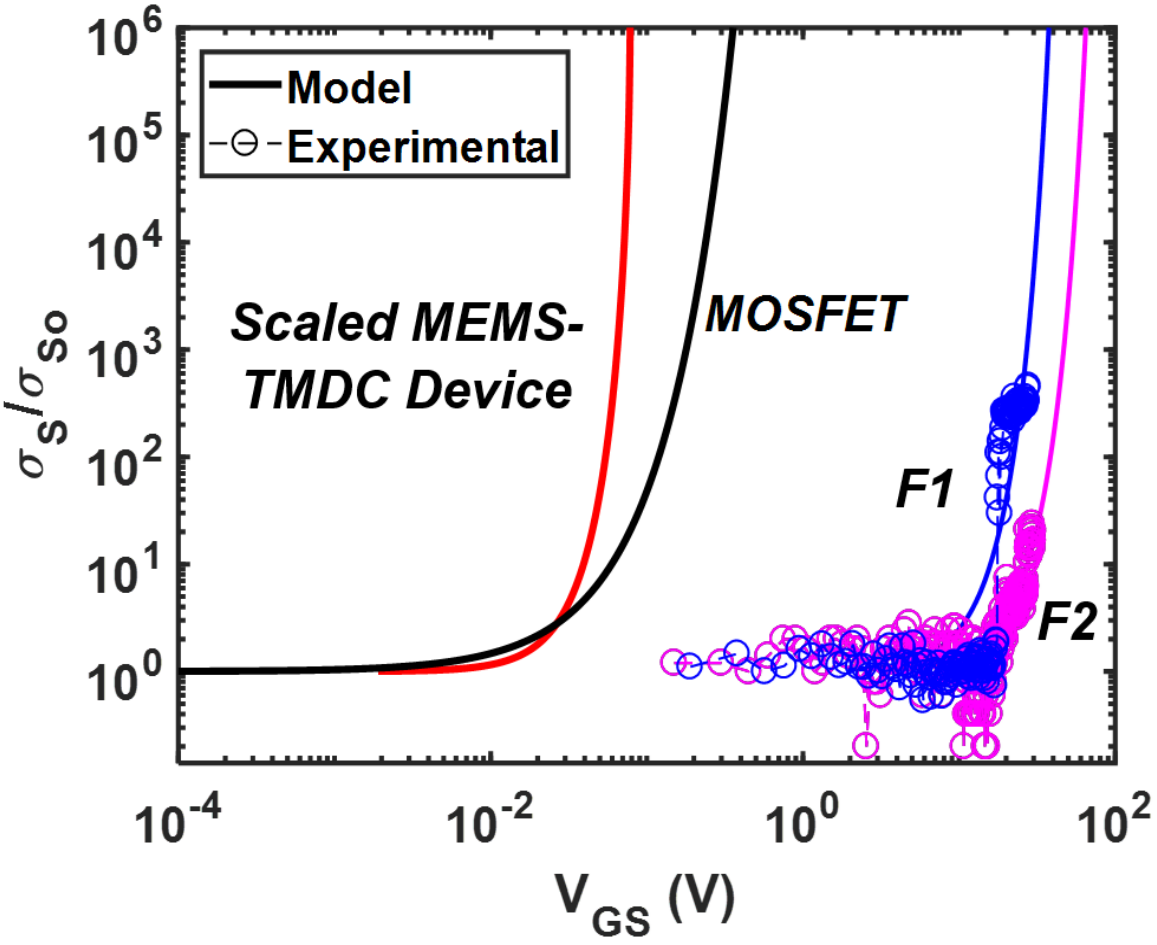

Figure 16: Measured (circles) and theoretical (solid lines) transfer characteristics of MEM-actuated TMDC devices. Red trace compares the transfer characteristics of a scaled MEMS-TMDC device to an ideal MOSFET (black trace).

Table 1: MEMS and TMDC dimensional and material parameters.

Parameter	Experimental		Theoretical	Units
2L-MoS_2 TMD				
ϕ_{dp}	-11.67		-11.67	eV/strain
Young Modulus (E_{TMD})	140		140	N/m^2 (x 10^9)
t_{TMD}	1.38		1.38	nm
k_{TMD}	193.2		193.2	N/m
Poly-$Si_{35}Ge_{65}$ MEM actuator				
Young Modulus (E_{SiGe})	152		152.0	N/m^2 (x 10^9)
L	73.0		20.0	μm
Lc	63.8		12.0	μm
L_D	3.0		1.0	μm
W	1.41		1.00	μm
t	1.00		1.50	μm
k_{CAN}	0.622		11.97	N/m
x_o	400		10.6	nm
V_{DS}	0.2		0.072	Volts
MEMS-TMDC Device	**Flake 1**	**Flake 2**		
W_{TMD}	100	300	10.6	nm
V_{GS}	28	31.5	0.072	Volts
σ_s/σ_{so}	400	20	10^6	dimensionless
ε_{TMD}	2.7	2.1	6.1	%

3.4 THEORETICAL CONDUCTIVITY VERSUS VOLTAGE TRANSFER CHARACTERISTICS

A force-balance model of the MEMS actuator, incorporating the MoS_2 flake as a spring, was created to predict the conductivity-voltage characteristic of the device as shown in Figure 17. In this model, the one end of the cantilever beam (which also serves as the current-conducting source electrode) is free to move laterally while the other end is fixed. The gate and drain electrodes are both fixed. (The fixed electrodes are shown in gray in Figure 17.) F_{CAN} and F_{TMD} are the spring restoring forces of the cantilever beam and the TMDC film, respectively. F_{VW1} and F_{VW2} are the van der Waals forces between the beam and the gate electrode and between the beam and the non-contacted and fixed electrode oppose the gate. F_E is the electrostatic force associated with the voltage applied between the gate and source, V_{GS}. It is noted that the electrostatic force induced by the voltage between the source and drain was determined to be insignificant compared to F_E due

to the much smaller area of the drain electrode compared to the gate. Additionally, the displacement of the cantilever beam required to strain the TMDC is much less than the displacement required for pull-in; hence, the device avoids stiction. Therefore, since there is no physical contact between the gate and beam, the adhesion forces are not included in the model. Finally, x_o is the both the length of the MoS_2 flake and gap between the gate and source (and drain and source) when the device is at equilibrium (unstrained). Based on this model, the force balance equation at steady state is given by

$$F_E = F_{CAN} + F_{TMD} + F_{VW_2} - F_{VW_1}. \qquad (16)$$

Note that F_{VW1} is subtracted on the right hand side of Equation (5) because it acts in the same direction as F_E, *i.e.*, it helps to induce tensile strain in the TMD film. However, the van der Waals forces are insignificant when $x_o > 15$ nm. Furthermore it is assumed that piezoelectric effects can be ignored because 2L-MoS_2 do not exhibit piezoelectricity [44]. Equation (16) is rewritten in terms of the dimensional, material and electrical parameters of the device but excluding the wan der Waals forces as follows:

$$\frac{\epsilon_o A V_{GS}^2}{2x_o^2(1-\varepsilon)^2} = k_{CAN} x_o \varepsilon + k_{TMD} W_{TMD} \varepsilon \qquad (17)$$

where $H = 4 \times 10^{-19}$ J is the Hamaker constant for SiGe, $\epsilon_o = 8.854 \times 10^{-12}$ F/m is the permittivity of free space, k_{CAN} is the effective stiffness of the cantilever, A is the actuation area, and V_{GS} is the voltage applied between the gate and source.

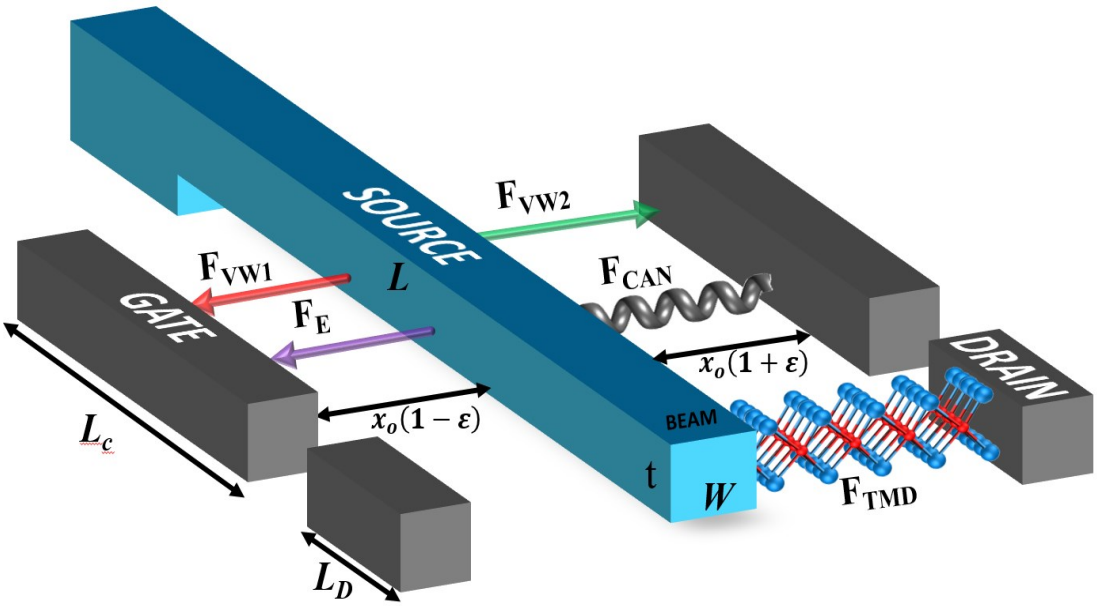

Figure 17: Force-balance model of the MEMS-TMDC device showing the various forces.

The MEM actuator was fabricated with a low-thermal-budget microfabrication process using polycrystalline silicon-germanium (poly-$Si_{0.35}Ge_{0.65}$) as the structural material (Young's modulus $E = 152\ GPa$) [13]. The effective stiffness of the cantilever beam is estimated using the following formula, which assumes a uniformly distributed load throughout the actuation length of the beam [10]:

$$k_{CAN} = \frac{2EW^3t}{3L^3}\left[\frac{3}{8-6(L_C/L)+(L_C/L)^2}\right] \text{(N/m)} \qquad (18)$$

where L is the total length of the beam, L_C is length of the portion of the beam in which the electrostatic force is applied, W is the beam width, and t is the thickness, as depicted in Figure 17. Using the parameters listed in Table 1 in Equation (18), the stiffness of the cantilever beam was determined to be $k_{CAN} = 0.622$ N/m. The stiffness of 2L-MoS_2 is $k_{TMD} = 193.2$ N/m, which is calculated by multiplying the Young's modulus (140 GPa) by the film thickness (1.38 nm) [37, 18, 45].

Using Equations (14) and (17), σ_S/σ_{S_O} can be solved numerically as a function of V_{GS} for a given value of x_o and W_{TMD}:

$$\sigma_S(V_{GS}) = \sigma_{S_O} \exp\left(-\frac{\phi_{dp}\varepsilon(V_{GS})|_{x_o,W_{TMD}}}{2kT}\right). \quad (19)$$

Using the values in Table 1 and W_{TMD} as the sole fitting parameter for each flake, Equation 8 is plotted in Figure 16. Reasonably good fits were achieved using W_{TMD} values of 100 nm and 300 nm for Flakes 1 and 2, respectively. The parameter W_{TMD} represents an effective width of the TMD since it was difficult to experimentally observe the structural integrity of the MoS_2 films or how well they were clamped across their width. The model predicts that a conductivity ratio of 10^6 should be achievable. However, experimentally the increase was limited to 400 due to either rupture of the MoS_2 film or slippage of the TMD film from the Cr/Au clamps. Nevertheless, these experimental results demonstrate the feasibility of exponential conductivity modulation in TMDC using a MEM actuator.

3.5 Switching Energy of Nanometer-Scaled Device

This section explores an energy-efficient means to induce strain in the TMDC flake to leverage the exponential dependence of TMDC conductivity on strain. The approach is to scale down the MEMS-TMDC device to the nanometer regime to take advantage of the van der Waals force (F_{VW1}) to assist in straining the TMDC.

First, a TMD is modeled as a massless spring with constant stiffness, k_{TMD} (N/m). Moreover, to simplify the analysis, the width of the TMD is assumed to be equal to its strain-free length, *i.e.*, $W_{TMD} = x_o$. Under these assumptions, the strain energy density in a TMD is

$$E_{TMD} = \frac{k_{TMD}\varepsilon^2}{2} \quad (20)$$

To ensure reliable operation (*i.e.*, high on/off current ratio over many switching cycles), the maximum strain induced in the TMD should be much lower than its ultimate tensile strain. Therefore, a large deformation potential (ϕ_{dp}) is desirable to lower the amount of strain needed to achieve a specified σ_S/σ_{S_O} ratio. Using Equation (15) a strain of $\varepsilon = 0.061$ is required to achieve $\sigma_S/\sigma_{S_O} = 10^6$ in 2L-MoS_2.

Substituting (15) into (20) gives E_{TMD} in terms of the TMD's stiffness, deformation potential, and on/off conductivity ratio:

$$E_{TMD} = \frac{2(kT)^2 k_{TMD}\left(\ln\sigma_S/\sigma_{S_O}\right)^2}{\phi_{dp}{}^2} \qquad (21)$$

Figure 18 plots E_{TMD} as a function of ϕ_{dp} for several TMD materials at room temperature, for a fixed value of $\sigma_S/\sigma_{S_O} = 10^6$. For example, 2L-$MoS_2$ has an energy density of $E_{TMD} = 0.38$ aJ/nm^2.

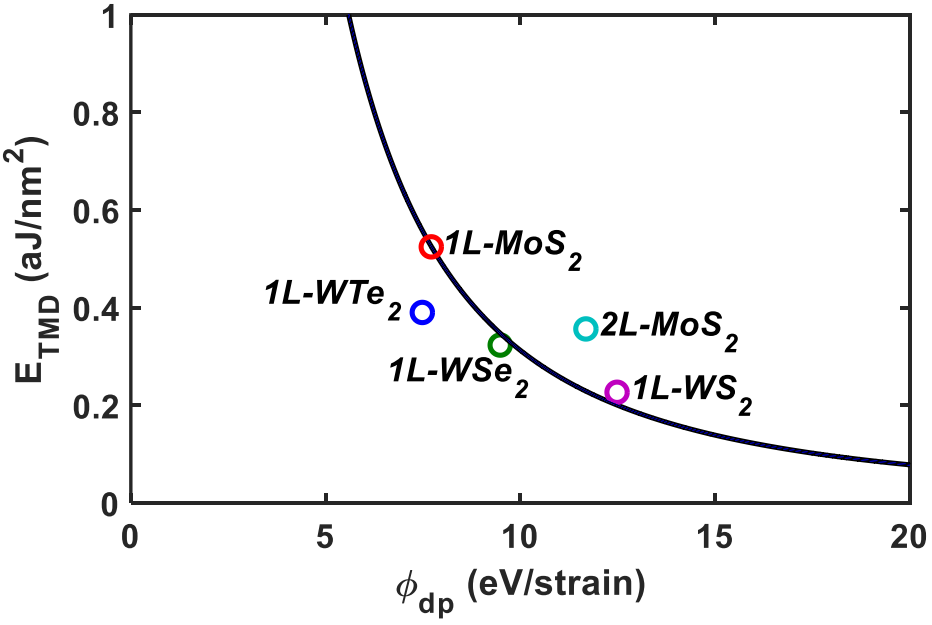

Figure 18: Strain energy density versus deformation potential for several TMD materials. The curve corresponds to k_{TMD} = 124.24 N/m.

As the MEMS-TMDC device is scaled to $x_o < 15$ nm the van der Waals forces (F_{VW1} and F_{VW2}) become increasingly significant. Therefore, the force-balance model should take these forces into account as follows,

$$\frac{\epsilon_o A V_{GS}^2}{2x_0^2(1-\varepsilon)^2} = k_{CAN} x_o \varepsilon + k_{TMD} x_o \varepsilon + \frac{HA_{VW}}{6\pi x_o^3(1+\varepsilon)^3} - \frac{HA_{VW}}{6\pi x_0^3(1-\varepsilon)^3} \qquad (22)$$

where $A_{VW} = (L_C + L_D)t$ is the effective area for the van der Waals forces. In order to achieve low switching-energy, the cantilever was designed such that k_{CAN} is ~10X smaller than k_{TMD}. This ensures that the total spring restoring force ($F_{CAN} + F_{TMD}$) is dominated by the TMD and the cantilever contributes negligible strain energy to the system. The dimensions of the cantilever are listed in the theoretical column of Table 1. This results in $k_{CAN} = 11.97$ N/m and $A = L_C t = 18$ μm^2. All the dimensions of the MEMS are kept constant except for x_o, which is the gap between the gate and source and length of the TMDC as shown in Figure 17.

The various forces and the electrostatic force required to induce $\varepsilon = 0.061$ ($\sigma_S/\sigma_{S_O} = 10^6$) in a 2L-$MoS_2$ flake are plotted in Figure 19 as a function of x_o. The green line represents F_E for an applied voltage of $V_{GS} = 0.072$ V. The black solid and dotted lines correspond to the spring restoring forces of the 2L-MoS_2 and cantilever beam, respectively. The red dotted line represents $-(F_{VW_2} - F_{VW_1})$, which increases as x_o is scaled down. The blue solid line represents the sum of the forces on the right hand side of Equation (16). When $x_o > 15$ nm, the spring restoring force of the TMDC is dominant and scales with x_o. However, the van der Waals forces increase according to $1/x_o^3$ and as the device is scaled down to x_o~15 nm, they become significant. This causes the sum of the forces on the right hand side of Equation (16) to decrease faster with decreasing x_o, as shown in Figure 19. The solution to Equation (16) occurs at the intersection between the blue and green lines, at $x_o = 10.6$ nm. This analysis serves to illustrate the benefit of van der Waals force to lower the switching energy of a MEM-actuated TMD switch.

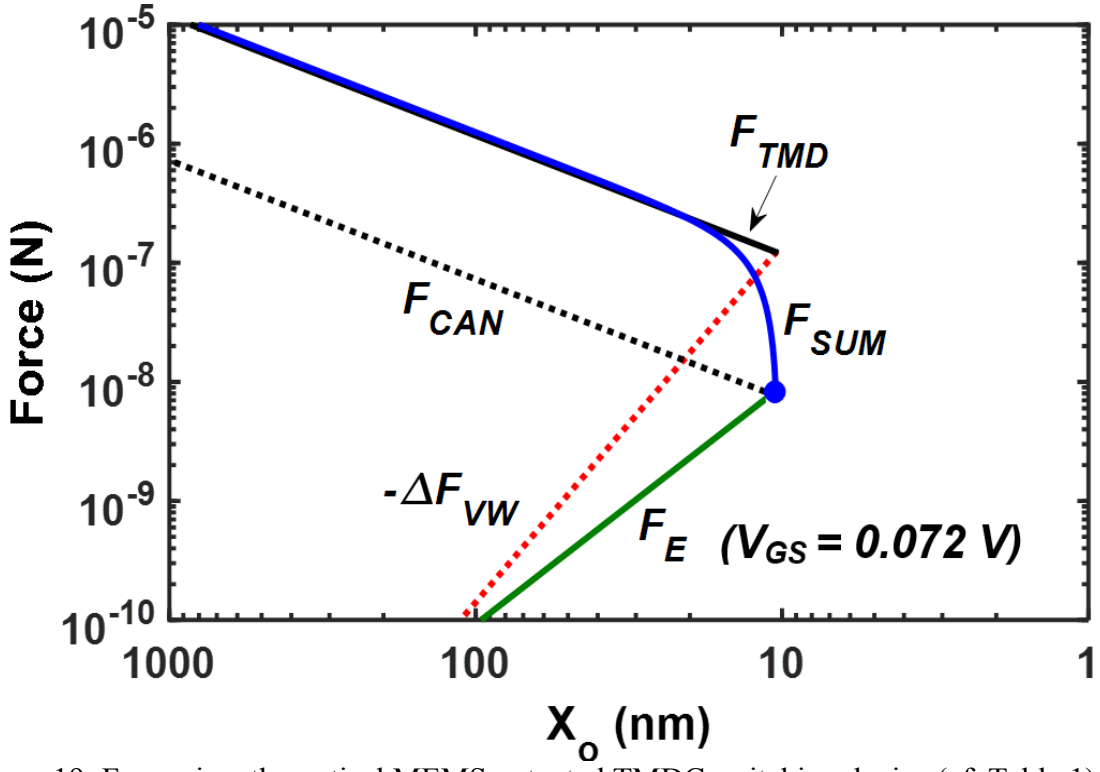

Figure 19: Forces in a theoretical MEMS-actuated TMDC switching device (cf. Table 1) as a function of x_o at a tensile strain of ε=0.061.

The strain energy E_M is calculated by integrating the force in Equation (16) over the distance traveled, from zero to the displacement needed to induce 6.1% strain (to achieve $\sigma_S/\sigma_{S_O} = 10^6$). The total electrical energy, E_T, needed to operate the MEMS actuator is calculated by adding the strain energy E_M to the electrical energy, E_E, needed to charge the plates . The energy densities are then calculated by dividing by the area of the TMDC layer, x_o^2, and are plotted in Figure 20 as a function of x_o. E_M is constant when x_o is large and is approximately equal to the strain energy density given above for the TMDC alone, $E_{TMD} = 0.38$ aJ/nm^2. However, when x_o is scaled below 15 nm, E_M decreases sharply due to the action of F_{VWI} to assist in straining the TMDC and reaches $E_M = 0.014$ aJ/nm^2 at $x_o = 10.6$ nm. The red solid line represents E_E, which also decreases sharply when x_o is scaled down below 15 nm and is approximately 25 times larger than E_M. The black dotted line represents the total energy density $(E_T = E_M + E_E)$.

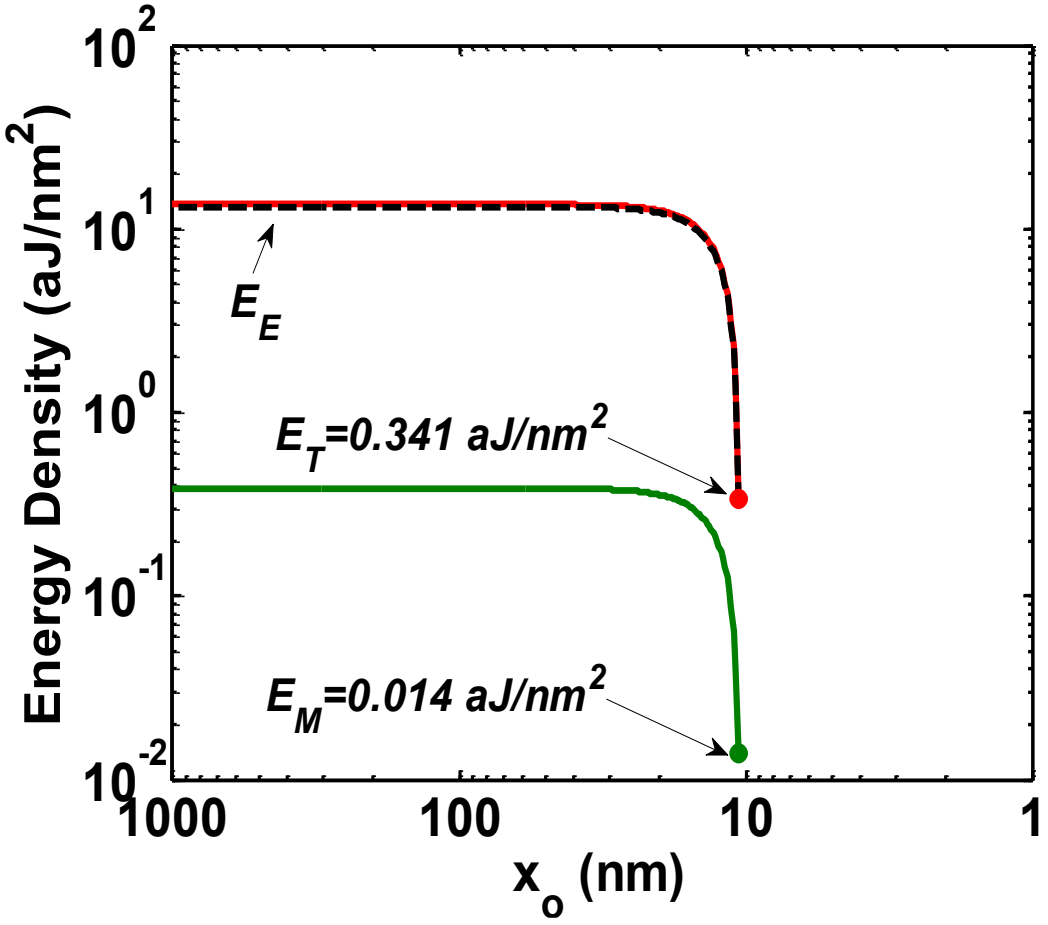

Figure 20: Switching energy density as a function of x_o. E_D decreases rapidly when x_o is scaled below 15 nm due to the action of F_{VWI}.

Finally, the calculated transfer characteristic of the MEMS-TMDC device with $x_o = 10.6$ nm (cf. Table I) is plotted (in red) in Figure 20, along with the ideal transfer characteristic of a MOSFET (in black). Note that the MEM-actuated TMD device exhibits steep switching behavior with an effective subthreshold swing of 17 mV/dec compared to 60 mV/dec for the MOSFET. Moreover, the device achieves $\sigma_S/\sigma_{S_O} = 10^6$ at $V_{GS} = 0.072$ V. The ideal resonant frequency of the MEMS-TMDC device was calculated to be ω_o=1.25 MHz, which was about four times higher than the MEMS alone, due to the high stiffness and low mass of the TMDC film.

It should be noted that fabricating such a device is challenging since it requires air gaps with aspect ratio $t/x_o = 150$. However, the world's leading dedicated semiconductor foundry (Taiwan Semiconductor Manufacturing Company, TSMC) have demonstrated that features with sub-15 nm gaps are possible, which are being manufactured in high volume today by using its 7 nm process technology [46]. Furthermore, self-aligned double patterning (SADP) and tilted ion implantation processing techniques can also be used to achieve sub-15 nm feature sizes [47, 48]. As well, deep reactive ion etching has been optimized to achieve aspect ratios of 120:1 in trenches of 35 nm [49], indicating the MEMS-TMDC device with actuation gap < 15nm can be fabricated using existing technologies.

3.6 New MEMS Actuator Design

As previously mentioned, pre-existing MEMS lateral actuators were used to strain the MoS_2 flakes. Since the MEMS actuator design was not specifically made to strain TMDC flakes, the overall fabrication yield was poor. As a result, this motivated us to design and fabricate new MEMS actuators to be able to control the TMDC strain more effectively at lower actuation voltages. The design and fabrication process of the new MEMS actuator and the experimental results were published in the MRS Advances Journal [50] and are presented in the next chapter.

Chapter 4: Exponential Conductivity Increase in Strained MoS_2 Using Comb- Drive MEMS Actuators

4.1 Introduction

Exploration of two-dimensional layered materials have tremendously increased over the past nine years, such as graphene and transitional metal dichalcogenides (TMDC) materials. These monolayers of TMDC materials have a weak interlayer van der Waals structure with strong covalent in-plane bonds [16]. In their monolayer form, TMDCs possess excellent in-plane mechanical properties, such as a high ultimate tensile strain of 11% [18]. These excellent mechanical properties permit the use of externally applied stress to influence their optical and electrical properties. One useful property is the large deformation potential (change in bandgap as a function of strain) that some TMDC materials possess. This is useful for strain-based sensors and for improving the performance of MoS_2 field-effect transistors [3- 9]. Recently, the large deformation potential exhibited by molybdenum disulfide (MoS_2) was proposed for low-energy switching [27, 28]. In this device, a MEMS actuator is predicted to uniaxially stretch a MoS_2 bi-layer flake up to 6% strain and increase its conductivity by six orders of magnitude with an applied gate voltage of 0.1 V, corresponding to an effective subthreshold swing of 17 mV/dec. As proof of concept, a SiGe MEMS cantilever was fabricated to strain MoS_2 flakes. Conductivity increases up to 400 were demonstrated corresponding to 2.7% strain. In this work, a comb-drive MEMS actuator was fabricated and used to strain a MoS_2 bi-layer flake to 3% resulting in a 3000 times increase in its conductivity.

4.2 Fabrication Process of Comb- Drive MEMS Actuators

A comb-drive MEMS actuator was designed to strain MoS_2 flakes and measure their conductivity. Figure 21(a) shows a schematic of the comb-drive actuator. The shuttle is able to

move up and down using four folded springs which have an effective stiffness of ~10% of the stiffness of the MoS_2 flake. A MoS_2 flake is placed and anchored between the moveable shuttle and fixed terminal as shown in Figure 21(a). Eight pairs of combs are used to move the shuttle upward when a voltage is applied between fixed gate and source terminals. This stretches the MoS_2 flake. To measure conductivity, a small constant voltage is applied between the drain and source (across MoS_2 flake) and the current is measured.

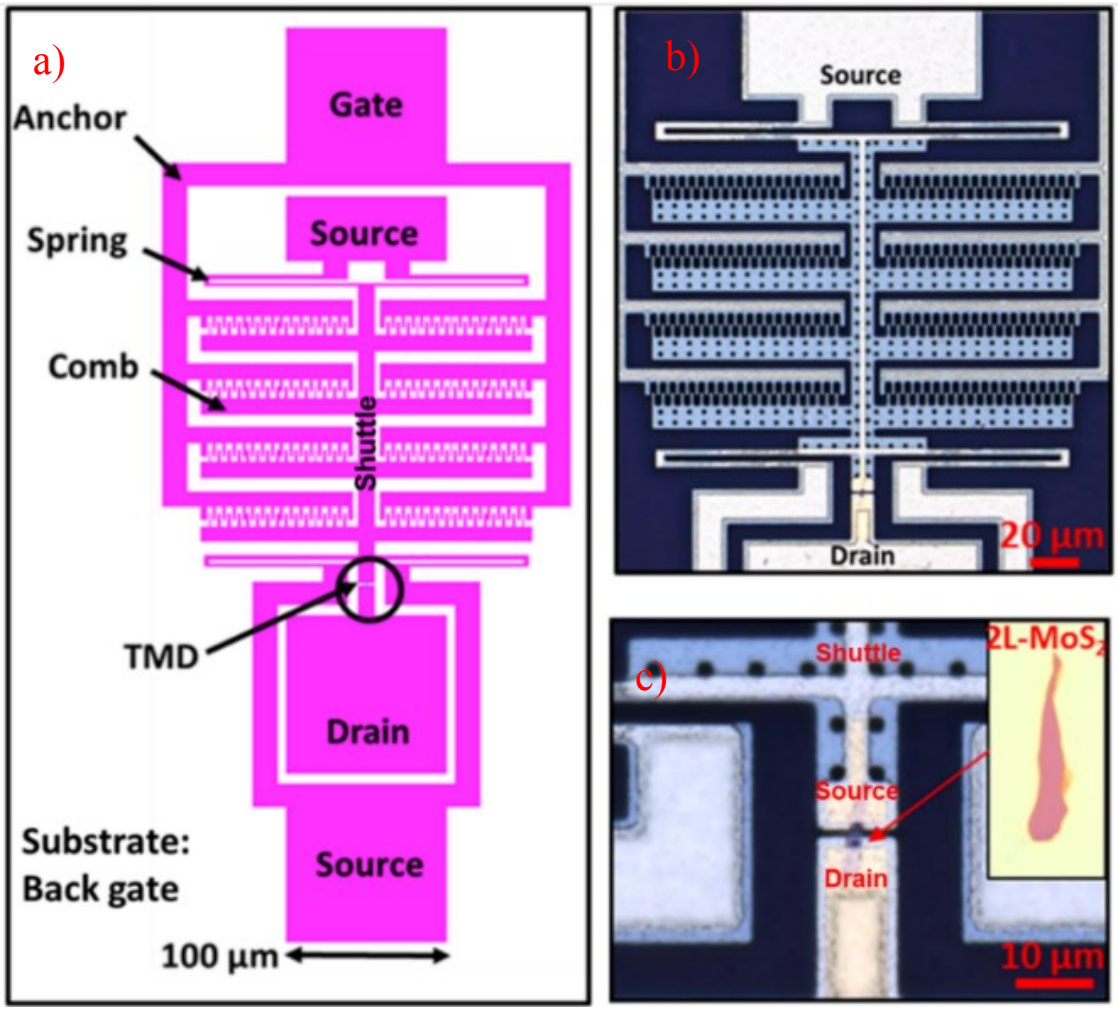

Figure 21: (a) Schematic diagram of MEMS-TMDC actuator. Optical micrographs of a fabricated MEMS-TMDC actuator at (b) 20X and (c) 50X magnification. Inset of (c) shows a 2L MoS2 flake on SiO2 at 100X

A CMOS compatible SiGe process was utilized to fabricate the MEMS actuators. The process contains 3 photo- and 1 e-beam- lithographic steps as shown in Figure 22. First, a layer of 80 nm thick aluminum oxide (Al2O3) was deposited by atomic-layer-deposition (ALD) onto a Si (100) wafer (Figure 22b)). This layer serves as an isolating layer for the device. Then a 300 nm low-temperature oxide (LTO) layer is deposited using low-pressure chemical vapor deposition at 400˚C. This layer serves as a sacrificial layer for the MEMS. The next step is to define regions where the SiGe will be anchored to the ALD layer. This is achieved by using the first photolithographic step to etch regions of LTO and leave the ALD exposed (Figure 22(c)). Then boron-doped polycrystalline silicon-germanium (poly-Si0.35Ge0.65) was deposited by LPCVD at 410˚C as the structural material (Figure 22(d)). The SiGe layer was then patterned using the second photolithographic step and an HBr/Cl2 etch (Figure 22(e)). A conformal layer of Ni is then deposited and patterned to serve as an electrode (Figure 22(f)).

MoS_2 flakes were obtained using mechanical exfoliation (scotch tape method) from a rock source and were transferred onto the MEMS actuator (Figure 22(g)). The number of layers was first verified using both Raman spectroscopy and color contrast between the flakes and 260nm SiO2/Si substrates. The MoS_2 flakes were then transferred to the MEMS actuator using Poly-methyl-methacrylate (PMMA) as the transfer medium. Mechanical clamping (and electrical contacting) of the MoS_2 flake was achieved by deposition and patterning of Ti/Au via electron beam deposition and e-beam lithography using a lift-off process (Figure 22(g)). Finally, the sacrificial LTO layer was selectively removed in anhydrous HF vapor to release the structure, as shown in Figure 22(h).

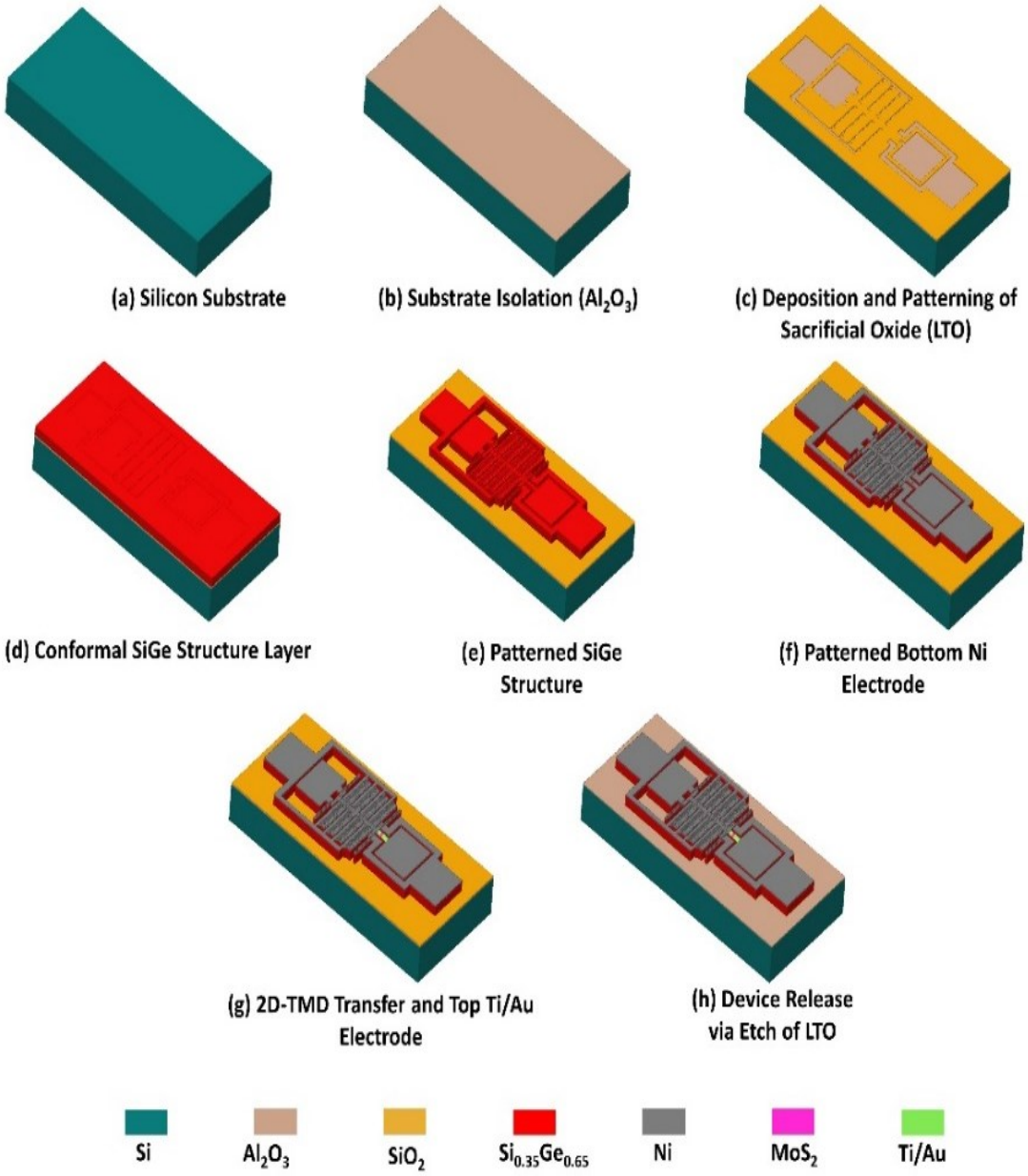

Figure 22: MEM actuator fabrication process.

4.3 ELECTRICAL CHARACTERIZATION

Optical images of the fabricated MEMS-TMDC device are shown at 20X and 50X magnification in Figure 21(b) and (c), respectively. The suspended MoS_2 bilayer flake is very thin and difficult to observe, however the inset of Figure 21(c) shows a 2L MoS_2 flake on a SiO_2 substrate at 100X.

During electrical actuation, it was discovered that vertical actuation of the shuttle occurred at much lower voltage (~4 V) compare to lateral actuation if a bias voltage was applied to the substrate as shown in Figure 23. Lateral actuation required ~80 V. This is due to the much larger area (and therefore capacitance) of the device in the out-of-plane direction compared to the in-plane direction. Therefore, the devices were actuated vertically to produce larger strain on the MoS_2 flake.

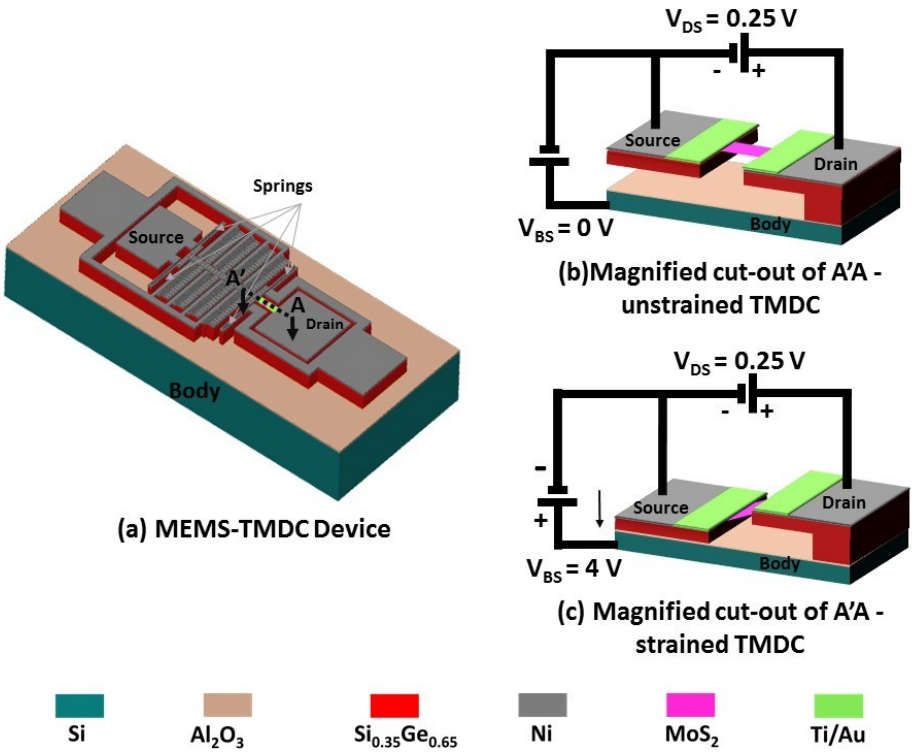

Figure 23: (a) Schematic diagram of the MEMS-TMDC device and a magnified cut- out view along A'A with the electrical measurement configuration with the TMDC (b) unstrained and (c) strained.

Figure 24(a) and (b) show a 3000 times increase in current in the MoS_2 flake when a voltage between the body and substrate was applied. Since the voltage between the drain and source was maintained at V_{DS}=0.25 V, this implies a three orders of magnitude increase in conductivity due to tensile strain. The change in conductivity is repeatable as shown in Figure 24(a) which plots 3 forward I-V characteristics. Figure 24(b) plots a forward and reverse I-V characteristic and reveals hysteresis behavior arising from the structure reaching pull-in and making contact with the bottom Al_2O_3 insulating layer. The current from the body to the source was also monitored to detect if any leakage was occurring. Figure 24(b) show that the leakage current, I_{BS}, was at or below the resolution limits of the measuring instrument ($<10^{-12}$ A).

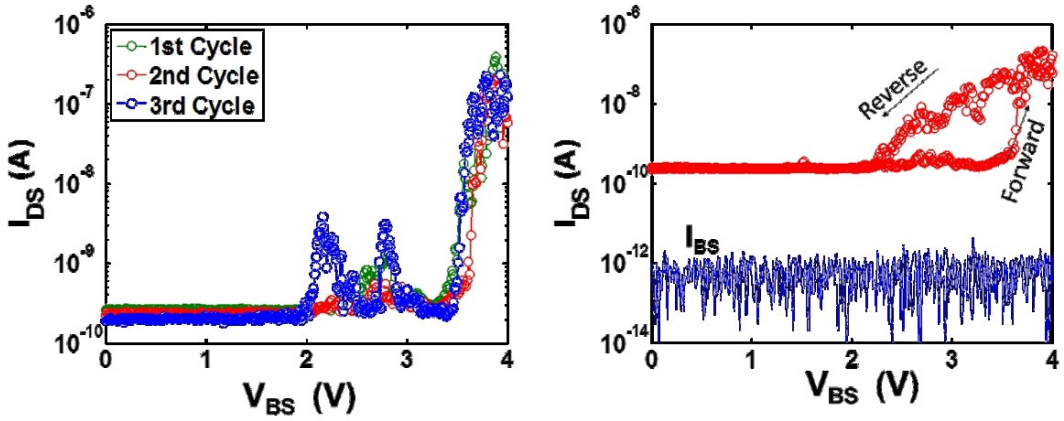

Figure 24: (a) I-V characteristic of MEM-TMDC device for three cycles. (b) I-V sweep demonstrating hysteresis behavior and leakage current at noise level.

4.4 2L-MoS_2 Strain Calculation

The conductivity of a 2-dimensional layer is dominated by the change in band-gap energy ΔEg according to the following formula,

$$\frac{\sigma_s}{\sigma_{so}} = e^{\left(\frac{-\Delta E_g}{2kT}\right)} \quad (23)$$

where k is the Boltzmann's constant, T is temperature, and σ_s and σ_{so} are the sheet conductivities under strain and no-strain, respectively. This is because the effect of strain on the effective mass and mobility of electrons is exponentially smaller [32]. Moreover, the band-gap energy is predicted to change linearly with applied strain according to

$$\Delta E_g = \phi_{dp}\varepsilon \quad (24)$$

where ϕ_{dp} is the deformation potential and ε is the strain. Combining, Equations (23) and (24) gives,

$$\frac{\sigma_s}{\sigma_{so}} = e^{\left(\frac{-\phi_{dp}\varepsilon}{2kT}\right)} \quad (25)$$

which shows that the conductivity changes exponentially with applied strain [28]. Figure 25 plots the predicted strain of MoS_2 bilayers as a function of conductivity ratio, σ_s/σ_{so}. Using the experimentally measured conductivity ratio of $\sigma_s/\sigma_{so} = 3000$ a maximum strain of $\varepsilon = 3.3\%$ is predicted.

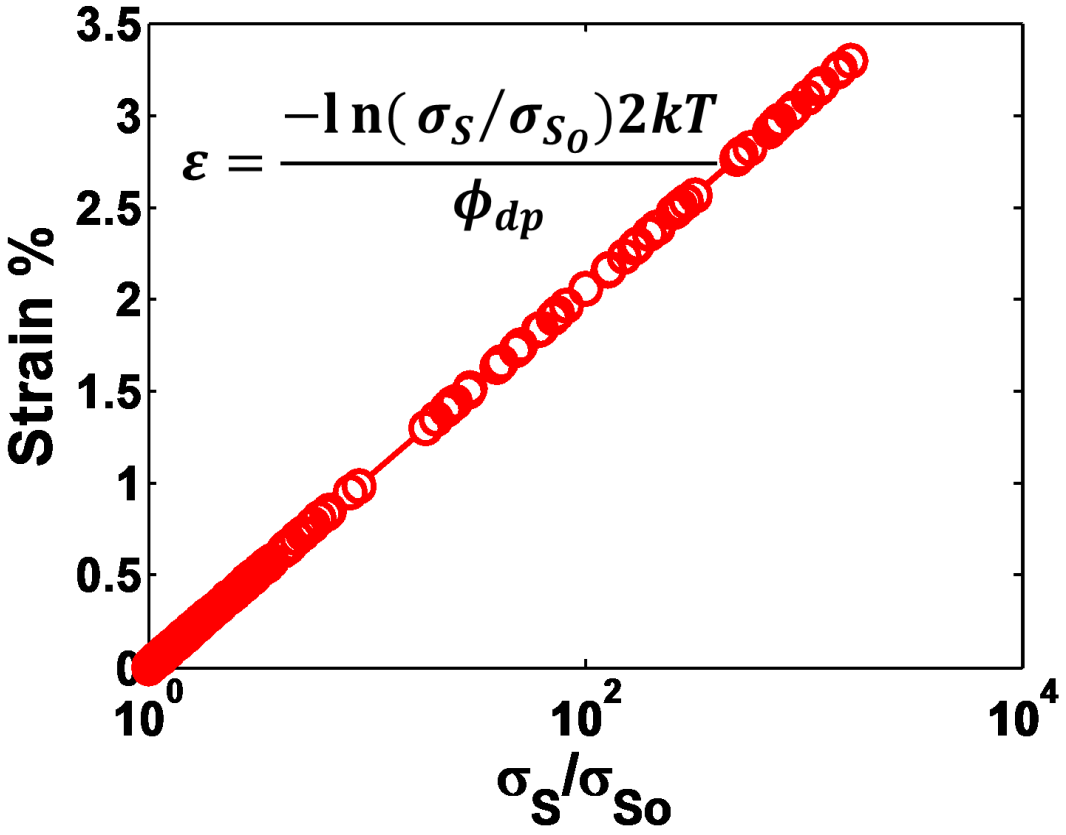

Figure 25: Strain percent as a function of experimental conductivity ratio in bilayer-MoS_2.

Additionally, a force balance model of the MEMS-TMDC was also used to calculate the strain in the MoS_2 flake:

$$F_E = F_{MEMS} + F_{TMD} \qquad (26)$$

where F_E is the electrostatic force induced by a voltage signal applied between the substrate and source (movable structure). F_{MEMS} and F_{TMD} are the spring forces of the folded flextures and the TMD film, respectively. In Equation (26), the young modulus of the TMDC can be represented as

the in-plane stiffness divided by its thickness, thus, Equation (26) can be expanded in terms of device parameters and material properties:

$$\frac{\epsilon_o A V_{Gs}^2}{2(g_o - x)^2} = k_{MEMS}(g_o - x) + k_{TMD} W_{TMD} \varepsilon \quad (27)$$

where the strain is defined as $\varepsilon = (l_f - l_o)/l_o$ and the final length, $l_f = \sqrt{l_o^2 + g_o^2}$. The distance $g_o = 0.30\ \mu m$ was determined by the amount of sacrificial LTO deposited discussed earlier in the fabrication process. The rest of the parameters in the model are shown in Table 2, where a combination of optical microscopy and a finite-element simulation software of the MEMS device were used. Using Equation (27) the strain vs voltage characteristic of the device was calculated as shown in Figure 26. The strain-voltage characteristic model agrees well with the experimental data.

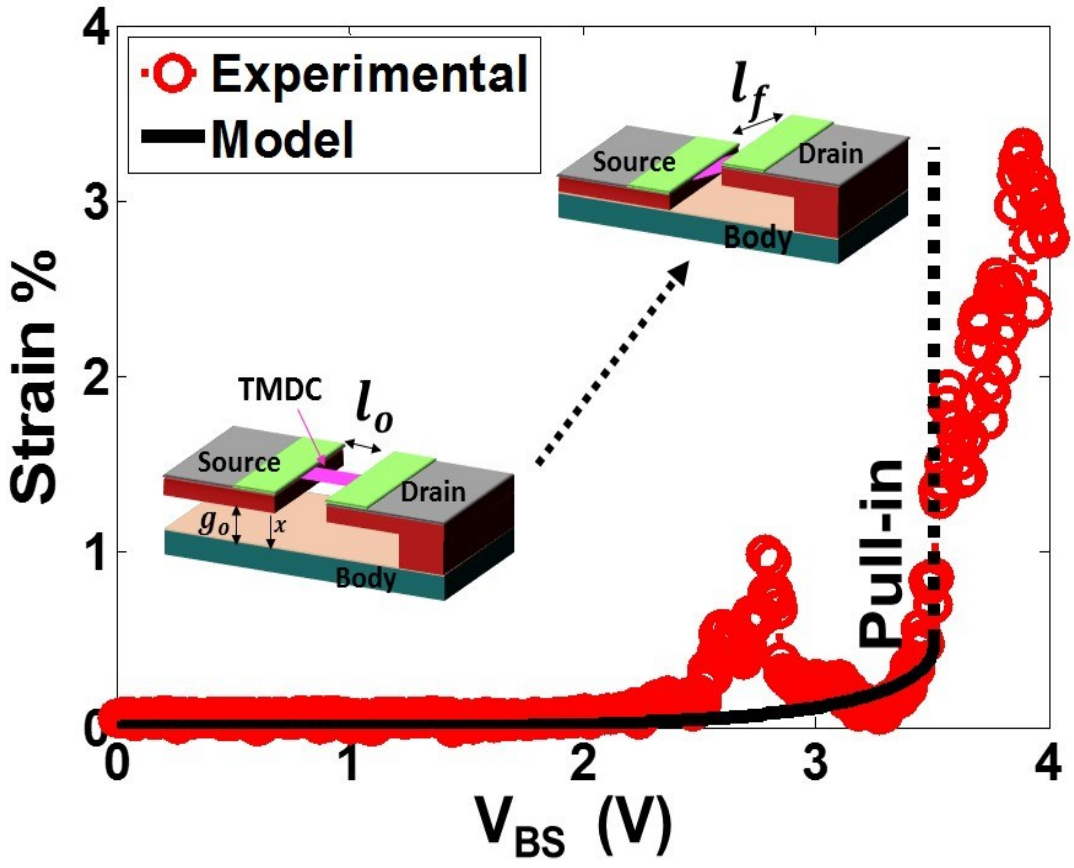

Figure 26: Strain as a function of body-source voltage. Experimental data and theoretical model matched closely.

Table 2: MEMS-TMDC parameters used for fitting.

Parameter	Experimental	Units
2L-MoS_2 TMD		
ϕ_{dp}	-11.67	eV/strain
Young Modulus (E_{TMD})	140	N/m^2 (x 10^9)
t_{TMD}	1.38	nm
k_{TMD}	193.2	N/m
W_{TMD}	3.5	μm
l_o	1.2	μm
Poly-$Si_{35}Ge_{65}$ MEM actuator		
Young Modulus (E_{SiGe})	152	N/m^2 (x 10^9)
A	9064	μm^2
k_{CAN}	86	N/m
g_o	300	nm
V_{DS}	0.25	Volts

Chapter 5: Conclusions and Future Work

The large deformation potential of MoS_2 in its -bi-layer form theoretically provides for large changes in conductivity, by up to six orders of magnitude, at tensile strain levels approximately one-half of their fracture point. Prototype cantilever MEMS-TMDC devices show increases in TMDC conductivity up to 400X in response to an applied gate voltage. The theoretical model matches the experimental data reasonably well, using an effective TMDC width as the sole fitting parameter. In principle, a MEMS actuator can be used to induce the tensile strain, with a strain energy density as low as 0.01 aJ/nm^2 for actuation gap size $x_o < 15$ nm due to van der Waals forces, with an actuation voltage below 0.1 V corresponding to an effective subthreshold swing of 17 mV/dec. Due to the poor yield during fabrication, this motivated us to design and fabricate new MEMS actuators to control the strain more effectively on the TMDC flakes at lower voltages.

As a result, poly-$Si_{0.35}Ge_{0.65}$ MEM comb-drive actuators with large out-of-plane actuation areas were fabricated successfully to specifically strain bi-layered MoS_2 flakes while simultaneously measuring electrical properties. Vertical actuation of the MEMS actuators provided strains up to 3.3% and an increase in TMDC conductivity by three orders of magnitude for several cycles. The theoretical model implemented also closely matched the experimental data. The amount of strain provided by the MEMS actuators was limited due to the small gap in the vertical direction.

To conclude, the large deformation potential and high ultimate tensile strain exhibited by bi-layered-MoS_2 allows for large changes in conductivity, demonstrating the ability to use MEMS-actuated TMDC devices for various applications including ultra-low power computing and strain based sensors. Currently, a new MEMS design is being designed to achieve higher conductivity (strain) changes in the TMDC at lower actuation voltages- and get closer to the low energy device (goal) as shown in Figure 27. Furthermore, new efforts are being made to fabricate the MEMS-TMDC device all in the same lab here at the University of Texas at El Paso.

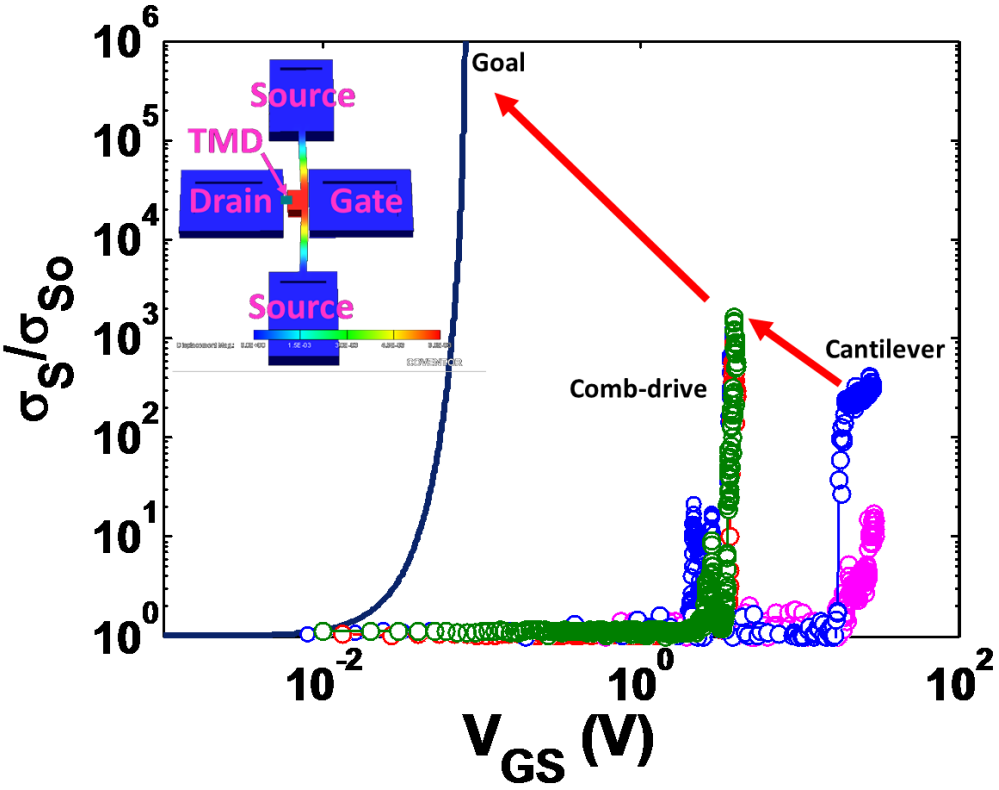

Figure 27: Conductivity ratio as a function of gate voltage for experimental devices and the final goal. Inset showing current MEM actuator design to provide higher strains to the TMDC at lower voltages.

References

[1] G. E. Moore, "Cramming more components onto integrated circuits," *Electronics,* vol. 38, pp. 114-117, 1965..

[2] B. Meyerson, *Semico Impact Conference,* Taiwan, 2004.

[3] U. E. Avci, D. H. Morris and I. A. Young, "Tunnel Field-Effect Transistors: Prospects and Challenges," *IEEE Journal of the Electron Devices Society,* vol. 3, no. 3, pp. 88-95, 2015.

[4] B. H. Calhoun, A. Wang and A. Chandrakasan, "Modeling and Sizing for Minimum Energy Operation," *IEEE JOURNAL OF SOLID-STATE CIRCUITS,* vol. 40, no. 9, pp. 1778-1786, 2005.

[5] P. Packan, "Device and Circuit Interactions," in *IEEE International Electron Device Meeting (IEDM '07) Short Course: Performance Boosters for Advanced CMOS Devices*, 2007.

[6] V. Pott, H. Kam, R. Nathanael, J. Jeon, E. Alon and T.-J. K. Liu, "Mechanical Computing Redux: Relays for Integrated Circuit Applications," *Proceedings of the IEEE,* vol. 98, no. 12, pp. 2076-2094, 2010.

[7] S. Kasap, "1.6 HEAT, THERMAL FLUCTUATIONS, AND NOISE," in *Principles of Electronic Materials and Devices Third Edition*, Boston, McGraw-Hill, 2006, pp. 40-45.

[8] "Center for Energy Efficient Electronics," [Online]. Available: https://www.e3s-center.org/research/. [Accessed 01 August 2017].

[9] T. N. Theis and P. M. Solomon, "It's Time to Reinvent the Transistor!," *Science,* vol. 327, no. 5973, pp. 1600-1601, 2010.

[10] A. V. Kshirsagar, D. S.P and G. S. A, "Design of MEMS Cantilever - Hand Calculation," *Sensors & Transducers Journal,* vol. 91, no. 4, pp. 55-69, 2008.

[11] I.-R. Chen, C. Qian, E. Yablonovitch and T.-J. K. Liu, "Nanomechanical Switch Designs to Overcome the Surface Adhesion Energy Limit," *Electron Device Letters,* vol. 36, no. 9, pp. 963-965, Sep 2015.

[12] S. Majumder, N. McGruer and G. Adams, "Adhesion and contact resistance in an electrostatic MEMS microswitch," in *18th IEEE International Conference* , 2005.

[13] S. A. Bhave, B. L. Bircumshaw, W. Z. Low, Y.-S. Kim, A. P. Pisano, T.-J. King and R. T. Howe, "Poly-SiGe: A high-Q structural material for integrated RF MEMS," in *Solid-State Sensors, Actuator and Microsystems Workshop*, 2002.

[14] R. Nathanael, V. Pott, H. Kam, J. Jeon and T.-J. K. Liu, "4-terminal relay technology for complementary logic," in *Electron Devices Meeting (IEDM)*, 2009.

[15] F. Niroui, A. I. Wang, E. M. Sletten, Y. Song, J. Kong, E. Yablonovitch, T. M. Swager, J. H. Lang and V. Bulovic, "Tunneling Nanoelectromechanical Switches Based on Compressible Molecular Thin Films," *ACS nano,* vol. 9, no. 8, pp. 7886-7894, Aug 2015.

[16] M. Chhowalla, Z. F. Liu and H. Zhang, "Two-Dimensional Transition Metal Dichalcogenide (TMD) Nanosheets," *Chem. Soc. Rev,* no. 44, pp. 2584-2586, 2015.

[17] P. Johari and V. B. Shenoy, "Tuning the Electronic Properties of Semiconducting Transition Metal Dichalcogenides by Applying Mechanical Strains," *ACS NANO,* vol. 6, no. 6, p. 5449–5456, 2012.

[18] S. Bertolazzi, J. Brivio and A. Kis, "Stretching and Breaking of Ultrathin MoS2," *ACS nano,* vol. 5, no. 12, pp. 9703-9709, Nov 2011.

[19] H.-Y. Chang, S. Yang, J. Lee, L. Tao, W.-S. Hwang, D. Jena, N. Lu and D. Akinwande, "High-performance, highly bendable MoS2 transistors with high-k dielectrics for flexible low-power systems," *Acs Nano,* vol. 7, no. 6, pp. 5446-5452, May 2013.

[20] S. J. Kim, S. Mondal, B. K. Min and C.-G. Choi, "Highly Sensitive and Flexible Strain–Pressure Sensors with Cracked Paddy-Shaped MoS2/Graphene Foam/Ecoflex Hybrid Nanostructures," *ACS Applied Materials & Interfaces,* vol. 10, no. 42, pp. 36377-36384, 2018.

[21] J. Lee, Z. Wang, K. He, J. Shan and P. X.-L. Feng, "High Frequency MoS2 Nanomechanical Resonators," *ACS Nano,* vol. 7, no. 7, pp. 6086-6091, 2013.

[22] N. Morell, A. Reserbat-Plantey, I. Tsioutsios, K. G. Schädler, F. Dubin, F. H. L. Koppens and A. Bachtold, "High Quality Factor Mechanical Resonators Based on WSe2 Monolayers," *ACS Nano,* vol. 16, no. 8, pp. 5102-5108, 2016.

[23] M.-Y. Tsai, A. Tarasov, Z. R. Hesabi, H. Taghinejad, P. M. Campbell, C. A. Joiner, A. Adibi and E. M. Vogel, "Flexible MoS2 Field-Effect Transistors for Gate-Tunable Piezoresistive Strain Sensors," *ACS Applied Materials & Interfaces,* vol. 7, no. 23, pp. 12850-12855, 2015.

[24] J. Qi, Y.-W. Lan, A. Z. Stieg, J.-H. Chen, Y.-L. Zhong, L.-J. Li, C.-D. Chen, Y. Zhang and K. L. Wang, "Piezoelectric effect in chemical vapour deposition-grown atomic-monolayer triangular molybdenum disulfide piezotronics," *Nature communications,* vol. 6, no. 7430, Jun 2015.

[25] S. B. Desai, S. R. M. M. Amani, D. Kiriya, M. Hettick, M. Tosun, Y. Zhou, M. Dubey, J. W. A. III, D. Chrzan and A. Javey, "Gold-Mediated Exfoliation of Ultralarge Optoelectronically-," *Advanced Materials,* vol. 28, pp. 4053-4058, 2016.

[26] S. Almeida, "Monolayer strain by NEMS for low power application," in *Energy Efficient Electronic Systems (E3S), 2015 Fourth Berkeley Symposium*, Berkeley, 2015.

[27] S. F. Almeida, D. Zubia, A. I. Vidaña and M. Martinez, "Conductance modulation in 2D materials by NEMS for lower-power applications," in *2017 Fifth Berkeley Symposium on Energy Efficient Electronic Systems & Steep Transistors Workshop (E3S)*, Berkeley, 2017.

[28] A. Vidana, D. Zubia, M. Martinez, E. Acosta, J. J. Mireles, T.-J. King and S. Almeida, "Conductivity modulation in strained transition-metal-dichalcogenides via micro-electro-mechanical actuation," *IOP Semiconductor Science and Technology,* vol. 34, no. 4, pp. 1-8, 2019.

[29] Y. Chai, S. Su, D. Yan, M. Ozkan, R. Lake and C. S. Ozkan, "Strain Gated Bilayer Molybdenum Disulfide Field Effect Transistor with Edge Contacts," *Nature Scientific Reports,* vol. 7, no. 41593, pp. 1-9, 2017.

[30] M.-Y. Tsai, A. Tarasov, Z. R. Hesabit, H. Taghinejad, P. M. Campbell, C. A. Joinert, A. Adibi and E. M. Vogel, "Flexible MoS2 Field-Effect Transistors for Gate-Tunable Piezoresistive Strain Sensors," *ACS Applied Materials & Interfaces,* vol. 7, no. 23, pp. 12850-12855, 2015.

[31] W. S. Yun, S. W. Han, S. C. Hong, I. G. Kim and J. D. Lee, "Thickness and strain effects on electronic structures of transition metal dichalcogenides: 2H-M X 2 semiconductors (M= Mo, W; X= S, Se, Te)," *Physical Review B,* vol. 85, no. 3, p. 033305, 2012.

[32] S. Yu, H. D. Xiong, K. Eshun, H. Yuan and Q. Li, "Phase transition, effective mass and carrier mobility of MoS2 monolayer under tensile strain," *Applied Surface Science,* vol. 325, pp. 27-32, Nov 2015.

[33] B. Radisavljevic, A. Radenovic, J. Brivio, V. Giacometti and A. Kis, "Single-layer MoS2 transistors," *Nature nanotechnology,* vol. 6, no. 3, pp. 147-150, Jan 2011.

[34] S. Das, H.-Y. Chen, A. V. Penumatcha and J. Appenzeller, "High performance multilayer MoS2 transistors with scandium contacts," *Nano letters,* vol. 13, no. 1, pp. 100-105, Dec 2012.

[35] W. Cao, J. Kang, W. Liu and K. Banerjee, "A compact current–voltage model for 2D semiconductor based field-effect transistors considering interface traps, mobility degradation, and inefficient doping effect," *Electron Devices, IEEE Transactions on,* vol. 61, no. 12, pp. 4282-4290, Dec 2014.

[36] W. S. Yun, S. W. Han, S. C. Hong, I. G. Kim and J. D. Lee, "Thickness and strain effects on electronic structures of transition metal dichalcogenides: 2H-M X 2 semiconductors (M= Mo, W; X= S, Se, Te).," *Physical Review B,* vol. 85, no. 3, p. 033305, Jan 2012.

[37] S. Manzeli, A. Allain, A. Ghadimi and A. Kis, "Piezoresistivity and Strain-induced Band Gap Tuning in Atomically Thin MoS2," *Nano letters,* vol. 15, no. 8, pp. 5330-5335, Jul 2015.

[38] N. Xu, J. Sun, I.-R. Chen, L. Hutin, Y. Chen, J. Fujiki, C. Qian and T.-J. K. Liu, "Hybrid CMOS/BEOL-NEMS Technology for Ultra-Low-Power IC Applications," in *IEEE International Electron Devices Meeting*, San Francisco, CA, 2014.

[39] M. Boukhicha, M. Calandra, M.-A. Measson, O. Lancry and A. Shukla, "Anharmonic phonons in few-layer MoS2: Raman spectroscopy of ultralow energy compression and shear modes," *Physical Review B,* vol. 87, no. 19, p. 195316, 2013.

[40] D.-H. Lien, J. S. Kang, M. Amani, K. Chen, M. Tosun, H.-P. Wang, T. Roy, M. S. Eggleston, M. C. Wu, M. Dubey, S.-C. Lee, J.-H. He and A. Javey, "Engineering Light Outcoupling in 2D Materials," *Nano Letters,* vol. 15, no. 2, p. 1356–1361, 2015.

[41] B. Radisavljevic, A. Radenovic, J. Brivio, V. Giacometti and A. Kis, "Single-layer MoS2 transistors," *Nature nanotechnology,* vol. 6, no. 3, pp. 147-150, 2011.

[42] E. Pensa, E. Cortés, G. Corthey, P. Carro, C. Vericat, M. H. Fonticelli, G. Benítez, A. A. Rubert and R. C. Salvarezza, "The Chemistry of the Sulfur–Gold Interface: In Search of a Unified Model," *Accounts of Chemical Research,* vol. 45, no. 8, p. 1183–1192, 2012.

[43] H. Häkkinen, "The gold–sulfur interface at the nanoscale," *Nature Chemistry,* vol. 4, pp. 443-455, 2012.

[44] J. Qi, Y.-W. Lan, A. Z. Stieg, J.-H. Chen, Y.-L. Zhong, L.-J. Li, C.-D. Chen, Y. Zhang and K. L. Wang, "Piezoelectric effect in chemical vapour deposition-grown atomic-monolayer triangular molybdenum disulfide piezotronics," *Nature communications,* vol. 6, no. 7430, 2015.

[45] P. Lu, X. Wu, W. Guo and X. C. Zeng, "Strain-dependent electronic and magnetic properties of MoS2 monolayer, bilayer, nanoribbons and nanotubes," *Physical Chemistry Chemical Physics,* vol. 14, pp. 13035-13040, 2012.

[46] S.-Y. Wu and e. al., "A 7nm CMOS platform technology featuring 4th generation FinFET transistors with a 0.027um2 high density 6-T SRAM cell for mobile SoC applications," in *2016 IEEE International Electron Devices Meeting (IEDM)*, San Francisco, 2016.

[47] A. Yeoh and e. al., "Interconnect Stack using Self-Aligned Quad and Double Patterning for 10nm High Volume Manufacturing," in *2018 IEEE International Interconnect Technology Conference (IITC)*, Santa Clara, 2018.

[48] P. Zheng, S. W. Kim, D. Connelly, K. Kato, F. Ding, L. Rubin and T.-J. King Liu, "Sub-lithographic patterning via tilted ion implantation for scaling beyond the 7 nm technology node," *IEEE Transactions on Electron Devices,* vol. 64, no. 1, pp. 231-236, 2017.

[49] J. Parasuraman, A. Summanwar, F. Marty, P. Basset, D. E. Angelescu and T. Bourouina, "Deep reactive ion etching of sub-micrometer trenches with ultra high aspect ratio," *Microelectronic Engineering,* vol. 113, pp. 35-39, 2014.

[50] A. Vidana, S. Almeida, M. Martinez, E. Acosta, J. Mireles, T. King and D. Zubia, "Exponential Conductivity Increase in Strained MoS2 via MEMS Actuation," *MRS Advances,* pp. 1-8, 2019.

Vita

Aldo Ivan Vidaña was born in Ciudad Juarez, Mexico. He attended Colegio Bilingue Alex for elementary and middle school. Then attended and graduated from Americas High School in 2010. He obtained his B.S. in Metallurgical and Materials Engineering from the University of Texas at El Paso in 2015 and graduated as the Undergraduate Student Marshall for the College of Engineering. During his undergraduate career he worked as an engineering ambassador, pre-calculus peer leader, undergraduate research assistant, and undergraduate teaching assistant. He performed an REU in Santa Barabara, CA and also in Grenoble, France at the prestigious laboratory CEA-Leti. He was also involved in several school organizations where served as the president for the Tau Beta Pi Honor Society.

He then decided to pursue his Master's in Electrical Engineering under the supervision of Dr. Zubia. He is currently working as a graduate research assistant in the NanoMIL laboratory at UTEP. He began working with a new project as part of the Center for Energy Efficient Electronics Science (E3S) consisted of five world-class academic institutions. This is where he began investigating bandgap modulation caused by mechanical strain in 2D materials for ultra-low power applications and strain-based sensors. As part of the center, intensive collaboration was done on a regular basis and resulted in two multi-institutional publications. As part of the project, a new device had to be designed, fabricated, and characterized using a variety of different tools in which he spent a total of 2 semester at UC Berkeley.

Contact Information: aldovidana@gmail.com

This thesis was typed by Aldo Ivan Vidaña